BEHAVIOR OF A POLYDISPERSE CLUSTER OF DROPS EVAPORATING IN A VORTEX

K. Harstad and J. **Bellan***
Jet Propulsion Laboratory
California Institute of Technology
Pasadena, CA 91109
U.S.A.

*corresponding author

ABSTRACT

A model has been developed to describe the dynamics and evaporation of polydisperse co]] ecti ons of liquid drops in an axisymmetric, infinite, cylindrical vortex. This formulation is valid both in the dense regime, where interactions between particles are important, and in the dilute regime, where interactions between particles are not important,

In contrast to the standard way of discretizing polydisperse collections of particles, where the initial size distribution is partitioned into a finite number of bins and these bins are fixed during the calculation, here it is only the initial size distribution which is partitioned into a finite number of sizes. Each initial size class thus defined is followed dynamically and thermodynamically in its own system of coordinates which moves with the drops. Therefore, each initial size class develops a continuum of sizes as the drops are centrifuged towards the hotter ambient and evaporate. The gas phase is followed in its own system of coordinates,

Because larger drops experience a larger centrifugal force, they approach the hotter arnbi ent faster, and depending upon the characteristic liquid heat-up time, they might evaporate faster. Thus, in this situation there is no longer a differential centrifugation by sizes as it was observed and calculated by other investigators in cold flow situations. Instead, the drop size distribution is nonmonotonic versus the radial coordinate in the vortex.

The centrifugal motion results in the formation of an inner vortex core devoid of drops and a cylindrical shell containing all the drops.

Results obtained from calculations made with this mode] show that dense collections of drops have more control parameters than dilute collections of drops. The most important control parameters are as follows: The inner region of the cluster and vortex are controlled by the air/liquid mass ratio and by the irrotational motion of the gas, whereas the outer region is controlled by the drop size distribution and by the solid body rotation of the gas. Considering the motion of the drops as an entity, the initial solid body rotation controls the drop number density distribution, the drop size distribution and the gas temperature within the cluster. It is shown that polydispersity increases the maximum mass fraction of the evaporated compound and enhances penetration of the evaporated compound into the ambient. Except for dilute clusters of drops, there seems to be no support for the previously-made assumption that the drop number distribution is uniform within the cluster. The drop size distribution is never uniform within the cluster after the initial time, even if the initial size distribution is monodisperse and the drop number distribution is uniform. This is the result of the screening effect of the drops located at the cluster peripheries which interfere with heat conduction and heat convection to the drops located within the central part of the cluster.

1. INTR ODUCTION.

Particle - laden flows are of interest both from an engineering point of view since they are encountered in many practical processes, and from a fundamental point of view since they occur in many natural phenomena. Example of the former are combustion devices using fuel sprays (Diesel engines, turbines, furnaces), and examples of the latter are tornadoes, dust storms and dust devils. What is of interest in studies of the practical processes is the ability to control them, whereas what is of interest in studies of the natural phenomena is to predict their behavior as a function of time. In both cases, a prerequisite to the ultimate goal is the understanding of the interaction between particles and flow, and, in certain situations, an understanding of the interaction between particles.

In many situations, the interaction between particles is not important. This is the case when the particles are so distant from each other that for all practi cal purposes they do not feel the presence of all other particles. The relevant parameter which quantifies this effect is the average distance between the centers of adjacent particles divided by the average diameter of the particles. If this parameter is very large, the particles do not interact between themselves and this situation is called the dilute limit; if this parameter is of order ten, particle interactions become important and this situation is called the dense limit. The present study will in particular define this parameter for polydisperse collections of drops. In previous rnonodisperse particle studies (Bellan and Cuffel, 1983), this quantity was called "the nondimensional radius of the sphere of influence".

The interaction between particles and flow assumes different characteristics depending upon both the mass loading and the nondimensional radius of the sphere of influence.

When the mass loading is low and the value of the nondimensional radius of the sphere of influence is large, the flow affects the particles but the particles do not affect the flow, and particle interactions are not important. This situation was studied experimentally and analytically by many investigators. Particle dispersion in a plane, turbulent free shear layer has been studied by Lazaro and Lasheras (1989) who showed that for nonevaporative water droplets the shear layer selectively disperses particles by sizes. The central inner region contains the small size particles, whereas two external sublayers were observed which had much larger particle sizes. Further studies of Lazaro and Lasheras, of an unforced (1992a) and forced (1992b) turbulent, plane mixing layer revealed that large scale coherent structures play a critical role in the dispersion of the particles, and that there is an optimum particle size for which lateral dispersion is maximized.

The differential and optimal dispersion of particles by organized, large coherent structures has also been described by Crowe, Chung and Troutt (1988), by Chung and Troutt (1988) and by Crowe, Chung and Troutt (1993). Particle dispersion was shown to be controlled by the Stokes number, St, of the particles, which is the ratio of the particle aerodynamic time to the flow time. At Stokes numbers near unity, particles were shown to accumulate at the edge of the coherent structures of the mixing layer, a phenomenon which was called "the focussing effect", This new observation shows that the previously held view that turbulence tends to a homogenize a mixture, is incorrect. For small values of St it was shown that particles disperse at the same rate as the flow, whereas for large values of St, particles are flung outside the coherent structures and behave ballistically without having much time to interact with the flow.

Similar conclusions were reached by Squires and Eaton (1991) who studied heavy particles in an isotropically turbulent, statistically-stationary flow. Direct numerical simulations with a Stokes number of 0,075, 0,15 and 0.52 revealed that particles collect preferentially in regions of low vorticity and high strain rate, and that this tendency is most pronounced for the intermediary value of St = 0.15. “his clustering of drops yielded instantaneous particle number densities which were sometimes 25 times the mean calculated value. This tendency of particle clustering was interpreted by the authors as a tendency of turbulence to inhibit rather than enhance mixing. This conclusion is consistent with that of Crowe, Chung and Troutt (1993)..,

In another publication, Squires and Eaton (1990) performed similar calculations for light particles rather than heavy particles. An identical clustering effect was found. When the mass loading of the flow was increased, the results showed that an increasing fraction of the turbulence kinetic energy was attenuated. Increasing the mass loading of the flow not only increasingly attenuated the turbulence kinetic energy, but also changed the spatial energy spectra, as a larger fraction of the turbulence kinetic energy was found to exist in the high wave number regime relative to the low wave number, It was found that lighter particles also concentrate in the low vorticity, high-strain-rate area of the flow, however the ratio of the instantaneous particle number density to the mean value was much higher for lighter particles than for heavy particles. The result was that the turbulence field was modified differently by light particles than by heavier particles, because the heavier particles were more uniformly distributed throughout the domain. With increasing mass loading, the results showed that the clustering tendency in the low vorticity region decreased for light

particles, whereas it increased for heavy particles.

The modification of the turbulent flow by particles has also been studied by Parthasarathy and Faeth (1990a, 1990b) and by Schreck and Kleis (1993). The investigation of Parthasarathy and Faeth addressed the modulation of the flow by the particles in homogeneous, dilute situations and the dispersion of particles in self-generated homogeneous turbulence. Experiments were performed with spherical glass particles falling in a stagnant water bath. Comparisons between companion numerical simulations based upon stochastic methods and the experiments observations yielded only partial agreement. Schreck and Kleis (1993) investigated the effect of both glass particles and almost neutrally buoyant plastic particles on grid-generated turbulence in water flow. As the particle concentration was increased, it was observed that the dissipation of the turbulence energy was monotonically increasing. The increase in the dissipation rate was about twice as high for glass particles as for plastic particles. A single model based upon a slip velocity between phases failed to simulate this result. In agreement with the results of Squires and Eaton (1990), the measurements showed that the high wave number region of the turbulence energy spectrum is modified by the presence of the particles. It was also shown that the particles have the tendency to increase the isotropy of the flow.

The dynamics of glass particle beads of 55×10^{-3} cm diameter in a round jet was explored by Longrnire and Eaton (1992). In this study the particle-to-air mass loading was as high as 0,65, however because of the large density of glass, the particle number density was still small. The conclusion of this investigation agrees with that of Crowe, Chung, and Troutt (1993) for shear layers and wakes, in that particle dispersion is observed to be dominated

by the large-sale vertical turbulent structures. Clustering of particles is observed, each cluster traveling with a velocity comparable to that of the large-scale structures. Clustering seems to occur between vortex ring structures, and it is suggested that particles are pulled out of the vortex rings and pushed downstream of the vortex cores. When inside the vortices, particles do not effect a complete turn inside the flow, but instead exit the vortex laterally, forming "tails". Presumably, this occurs because of the large momentum of the glass beads which cannot be fully entrained by the vortex.

Other studies of particle-laden flows without particle interactions are those of Elghobashi and Truesdell (1992, 1993). The two-way interaction between particles and flow mentioned in Elghobashi and Truesdell (1993) is calculated only locally and it is limited to all the forces acting on an isolated particle, the negative of which acts on the flow. The continuity equation does not contain a source term due to presence of particles, as the volume fraction of the particles is less than 10^{3}.

High mass loadings of up to 0,90 were achieved by Hardalupas, Taylor and Whitelaw (1992), also with glass beads in an air flow, in the rather complex geometry of the vertical sudden step expansion in the direction of gravity. The observations, made over a range of air velocities, expansion diameter ratio and loading ratio, showed that the beads were dispersed by interaction with large scale eddies, just like in the studies described above. Experiments performed by Hardalupas, Taylor and Whitelaw (1990) in an unconfined burner with kerosene drops revealed that the drops were centrifuged by the existing swirl away from the center line and towards the edge of the spray, so that eventually a large proportion for the liquid could be found at the edge of the swirling jet.

All of theabove studies were rnadewith either low loading ratios or with low enough particle number densities, so that particle interactions were not important.

However, in many practical applications, particle interactions are important. One significant example is spray combustion, where the region around the atomizer contains such a dense collection of drops that precise measurement techniques to explore that region have been unavailable for a longtime. It is only very recently that appropriate diagnostics have evolved for investigating this dense spray region. Design engineers have known for a long time that it is precisely in this region that one finds the control parameters for process optimization. There is not doubt that in this region, near the atomizer, particle interactions become important. The experimental investigation of Zhang, Davis and Ruth (1993) of two interacting drops in the low Reynolds number regime (10^{-2}-10^{3}) show that dynamic interactions between drops both reduce the slip velocities of the drops with respect to the flow and change the trajectories of the drops. The interaction between drops becomes stronger with decreasing size ratio and drop separation, and increasing viscosity ratio between the liquids. In the intermediate Reynolds number regime Tal, Lee and Sirignano (1993) have shown, using a multisphere cylindrical cell model, that wake effects reduce considerably both drag and the Nusselt number. Since this analysis did not account for mass transfer and evaporation, or for internal heating of the drops, interaction effects are obviously underestimated. Two evaporating droplets moving in tandem were studied for Re = 0(100) by Raju and Sirignano (1990) who found significant departures from the isolated drop drag and Nusselt number for droplet spacings of 2-15 drop diameters for initial Reynolds numbers of 50-200. In particular, it was found that evaporation has an important

effect on the drag coefficient. All these results are valid for a small number of nteracting drops which means that screening effects associated with many body interactions are not taken into account.

Hydrodynamic interactions of a binary size suspension for an arbitrarily large number of particles has been simulated by Chang and Powell (1993). They used the concept of the inverse of the grand mobility matrix to calculate the many-body far-fields effects. As noticed by the authors, the grand mobility matrix cannot account for shielding effects, except locally, because it does not contain the reflections from spheres located far from the "test" sphere. To account for multiple reflections, the authors use the grand resistance matrix, which is the inverted grand mobility matrix. The grand resistance matrix has been shown by Durlofsky, Brady and Bossis (1987) to account for these shielding effects. Since this inverted grand mobility matrix, which is the many-body approximation to the resistance matrix, still lacks near field effects, because all multiple effects are not included, a correction is introduced which is called a lubrication effect. One interesting prediction of this model is the formation of particle clusters from an initial condition of randomly distributed particles. In these simulations the size ratio of the particles varied from 2 to 4, and the total number of particles never exceeded 100. In the cluster configuration, small particles were seen to fit between large particles resulting in binary size clusters of drops. These computational results are consistent with experimental findings in sprays (Mizutani et al. 1993; McDonnel, Adachi and Samulsen, 1992; Rudoff et al. 1989) showing that clusters of drops are an nherent feature of the spray, whether burning or not burning.

In this manuscript we present a model of a polydisperse cluster of evaporating drops in

a vertical flow. Multidrop interactions are taken into account both thermodynamically and dynamically using previously developed concepts for monodisperse clusters of drops. It is the concept of the sphere of influence for a "test" drop, as discussed above, which quantifies the extent of drop interactions. This concept has been previously defined for monodisperse collections of drops of Bellan and Cuffel, 1983 in a study of a stationary cluster of drops, and by Bellan and Harstad, 1990 in a study of monodisperse clusters of drops in a vertical flow where the drop motion was assumed to be self-similar. In the present study, the concept of sphere of influence is generalized for a polydisperse cluster. The important concept from the point of view of cluster dynamics is that of "porosity". The porosity describes the ability of flow to penetrate the cluster. Although the porosity is not an explicit parameter in this model, it is reflected in the modeling of the drag force which depends upon the drop number density as well as the evaporation rate. It is also reflected in the gradient of the pressure associated with the quasi-static interaction between drops and gas depending upon the liquid volume fraction which is a function of the drop number density.

In Section 2 we present a description of the exact configuration studied here, as well as of the important phenomena taken into account, The formulation of the model is described in Section 3, and the method of solution for the model equations is detailed in Section 4. The rationale used to prescribe the initial conditions is exposed in Section 5. Results obtained from the calculation are discussed and interpreted in Section 6. Finally, a summary of the results and salient conclusions are presented in Section 7.

2. DESCRIPTION OF THE PHYSICAL SITUATION ANI) ASSUMPTIONS.

The configuration studied here is that of an isolated, 2-dimensional, cylindrical vortex,

infinite in extent, which contains a cluster of drops. The drops in the cluster have a continuum of sizes and velocities varying with radius and time, however for the purpose of computation this will be approximated by a finite number of sizes at a finite set of radial positions. Figure 1 depicts a binary size distribution.

It is important to mention that in this formulation it is only the initial size distribution that is partitioned into distinct size classes. Once this is done, each size class is followed in time in a system of coordinates evolving with the initial size class. Since the drops evaporate while they are being dispersed by the vortex, each initial size class will evolve into a multitude of drop sizes. Because it is assumed that the dependent variables do not have an azimuthal dependence, the number of sizes evolving from each initial size class is the number of radial points (in the system of coordinates attached to the size class) chosen for the numerical solution . Thus, as the spatial resolution is increased, so is the number of sizes evolving from each size class, until the solution becomes invariant with the number of points chosen.

Note that, in contrast to previous studies, here the drops both disperse and evaporate, so that a selective dispersion by size might not occur. This is because if larger drops are initially centrifuged further out, they will be in contact with hotter gas and may evaporate faster than the smaller particles closer to the core. The particle size distribution will be a direct result of these two competing processes.

As the drops disperse, a slip velocity exists between drops and gas, and the dynamic interaction between drops and gas occurs through a drag force. This drag force is the result of shape-drag, friction and a contribution due to evaporation from the drops. This force was

modeled by Bellan and Harstad (1990) for monodisperse clusters of drops and was found to be proportional to the drop number density.

In this formulation, drag is associated with local small scale pressure gradients. However, the pressure change may be due to other effects as well, For this reason, on a large scale the pressure is considered to be the sum of several terms:

$$p = p_{amb} + \tilde{p} + p' + \hat{p} \qquad (1)$$

where p_{amb} is the ambient, constant pressure; $\tilde{p}$ is due to the centrifugal force on the gas; p' is the pressure due to convective changes in the radial gas velocity and it satisfies Bernouilli's relation

$$p' + \frac{1}{2} \rho_g u_{gr}^2 = p_s(t) \qquad (2)$$

and $\hat{p}$ is associated with the quasi - static interaction between drops and gas, that is $\nabla\hat{p}$ has a length scale much larger than the drop radius, R_d. Consider thus a drop located at the radial position r_p as shown on Fig.2. The net force on the drop in direction r is

$$F_{ds} = -\int \hat{p}_n \cos\theta \, dA \qquad (3)$$

where $dA = 2\pi R_d^2 \sin\theta \, d\theta$ is the ring area element and $\hat{p}_n$ is the normal pressure.

But

$$\hat{p}_n = \hat{p}(r_p) + (r - r_p) \frac{\partial \hat{p}}{\partial r}(r_p) + \text{higher order terms} \qquad (4)$$

and $r - r_p = R_d \cos\theta$ so that

$$F_{dB} = -\frac{4\pi}{3} R_d^3 \frac{\partial p}{\partial r} = -\frac{m_d}{\rho_l} \frac{\partial p}{\partial r} \quad (5)$$

One consequence of the drop azimuthal motion is the creation of small scale turbulent features. This phenomenon has not been yet modeled in detail as it represents a formidable task. In the present model, the result of this shear motion is globally represented by a turbulent viscosity, μ_T, which is added to the laminar viscosity, μ_g

$$\mu_T = \rho_g A_T r_c |\vec{u}_s| \quad (6)$$

where ρ_g is the gas density, $A_T = C_T/Pr_g$ where C_T is a constant and Pr_g is the Prandtl number for the gas, r_c is the radial coordinate in the system associated with the gas in the cluster, and u, is the mean slip velocity relative to the gas. The mean value, u_s, is obtained by averaging over drop initial size classes, j, and drop number, N_{cj}, for each size class in the cluster gas coordinates with

$$\vec{u}_{sj} = \vec{u}_{dj} - \vec{u}_g \quad (7)$$

$$\vec{u}_s = \frac{\sum_j \vec{u}_{sj} N_{cj}}{\sum_j N_{cj}} \quad (8)$$

where $\vec{u}_{sj}$ is the slip velocity for initial size j; $\vec{u}_{dj}$ is the drop velocity for initial size class j and $\vec{u}_g$ is the gas velocity. The value of C_T is a parameter of the problem and the model's sensitivity to it will be studied as part of this investigation.

The drops centrifugation results in the formation of a relatively thick drop shell inside the vortex. Thus, the cluster, formed by the drops and the gas in that shell, exchanges mass, species, momentum and energy with the gas devoid of drops in the vortex though an inner

and an outer boundary. For the gas surrounding the cluster, the cluster appears to a certain extent as a porous material where the drops represent the condensed phase. Thus the surrounding gas cannot easily penetrate the cluster. Notice that since the cluster does not have a solid boundary with the ambient gas, there is limited shear at the cluster boundary. This is to say that no exceptionally large velocity gradients are expected near the boundaries; however, relatively large gradients in the mass fractions and temperature might exist, Thus, the effect of the turbulent viscosity is taken into account in the gas species equation through the Schmidt number, Sc, and in the gas energy through the Prandtl number, but an equivalent term does not exist in the gas momentum equation.

Consistent with the above approach, the heat transfer "interaction between the cluster and outer gas is treated using a Nusselt number (Nu_c) approach, where the following expression is chosen for Nu_c

$$Nu_c = 1 + C_1 Pr_g \left| \frac{r_c \rho_g \max(0, u_{sr})}{\mu_g + \mu_T} \right|_{r_c = R_c} \qquad (9)$$

where C_1 is a constant which will be treated in this study as a parameter and u_{sr} is the radial component of u_s. The gas temperature and mass fractions in the surrounding of the cluster arc assumed to diffuse towards the cluster from a prescribed value at infinity.

3. FORMULATION OF THE MODEL

Since the novelty of this work is in the polydisperse representation, this part of the model will be described in detail. The previously developed model of the evaporation of a drop in its own sphere of influence (Bellan and Cuffel, 1983; Bellan and Harstad, 1988) is used here as an element of the model. For a monodisperse, uniformly distributed collection

of drops, the sphere of influence of each drop (Bellan and Cuffel, 1983) is centered at the drop center and has a radius, R_j, which is the half distance between the centers of adjacent drops. For a polydisperse, nonuniformly distributed collection of drops, an averaging is performed both over the distance from a test drop to the surrounding drops and over the size of the drops surrounding the test drop, as will be shown below.

A. -Conservation Equations for the Drops. In the present formulation, j labels a set of drops based upon an initial size. Class j is not a size class since there may be particles coming from other classes which may have at time t and location r_c the same size as the j particles, due to the centrifuging effect discussed above. Each class has Lagrangian radial coordinates associated with it, $r_j^{(k)}(t)$ where k identifies the discretization of the vortex into rings corresponding to intervals $(r_j^{(k)}, r_j^{(k+1)})$. Any dependent quantity can be averaged in such an interval as follows

$$\int_{r_j^{(k)}}^{r_j^{(k+1)}} V(r)\, r\, dr = 0.5 \left\{ [r_j^{(k+1)}]^2 - [r_j^{(k)}]^2 \right\} \bar{V} \qquad (1ea)$$

$$\text{where } \bar{V} = V[r_j^{(k+1/2)}] \equiv V^{(k+1/2)} \qquad (10b)$$

and

$$r_j^{(k+I/2)} = \sqrt{0.5 \left\{ [r_j^{(k)}]^2 + [r_j^{(k+1)}]^2 \right\}} \qquad (1OC)$$

The motion of the drops is the result of both conventional forces and turbulent diffusive effects. The diffusive effects are similar to those encountered when considering the Brownian motion of particles as discussed by Hidy and Brock, 1970. Thus, the change in the radial velocity of a drop of size class j due to this diffusion effect is assumed to be

$$\delta u_{drj} = -D_{drj} \frac{\partial}{\partial r} \left[\ln \left(\frac{n_j}{n_j^o} \right) \right] \qquad (11)$$

where n_j is the drop number density of class j, the superscript zero denoting the initial conditions. In Eq.(11)

$$D_{drj} = A_T \nu_{sj} (r_j)^2 \qquad (12)$$

which corresponds to the Stokes-Einstein formula with mean drop energy due to turbulence Of $A_T m_{dj} (V_{,j} r_{j\cdot})^2$. Here ν_{sj} is defined as a frequency associated with drag as in Bellan and Harstad (1990)

$$\nu_{sj} = \rho_g A_{dj} C_D |\vec{u}_{sj}| / (2m_{dj}) \qquad (13)$$

where A_d is the transverse area, C_D is the drag coefficient taken to have the same dependence upon the drop Reynolds number and evaporative blowing parameter as in Bellan and Harstad (1987) and Cliffe and Lever (1985), and m_d is the drop mass. Thus, for example, the conservation equation for the drop number density for each initial class j is in an Eulerian system of coordinates

$$\frac{\partial n_j}{\partial t} + \frac{1}{r} \frac{\partial}{\partial r} (r n_j u_{drj}) = 0 \qquad (14)$$

where. the diffusive velocity is taken into account in u_{drj}. The number of drops in class j, in the ring [k, k+ 1] is proportional to

$$N_j^{(k+1/2)} = \int_{r_j^{(k)}}^{r_j^{(k+1)}} n_j \, r \, dr \qquad (15)$$

and in Lagrangian coordinates Eq.(14) is equivalent to

$$dN_j^{(k+1/2)}/dt = 0 \qquad (16)$$

Note that $N_j^{(k+1/2)}$ are constants of motion. Once the values of $r_j^{(k+1/2)}$ are known, $n_j^{(k+1/2)}$ can be calculated from $N_j^{(k+1/2)}$ using Eq. (10).

Defining the angular momenta of drops and gas, respectively $\Gamma_{d0j} \equiv r_j u_{d0j}$ and $\Gamma_{g0} \equiv r u_{g0}$, the drops conservation equations are

$$dr_j^{(k)}/dt = u_{drj}^{(k)} \qquad (17)$$

$$du_{drj}^{(k)}/dt = [u_{d0j}^{(k)}]^2/r_j^{(k)} - \nu_{sj}^{(k)} \{u_{drj}^{(k)} - u_{gr}(r_j^{(k)})\} \qquad (18)$$

$$+ D_{drj}^{(k)} \left[\frac{\partial}{\partial r}\left(\frac{1}{r} \frac{\partial}{\partial r}(r u_{drj})\right) + \frac{\partial u_{drj}}{\partial r} \frac{\partial}{\partial r} \ln\left(\frac{n_j}{n_j^o}\right) \right]_{r=r_j^{(k)}}$$

$$- \frac{1}{\rho_1} \frac{\partial p}{\partial r}(r_j^{(k)})$$

$$d\Gamma_{d0j}^{(k)}/dt = - \nu_{sj}^{(k)} [\Gamma_{d0j}^{(k)} - \Gamma_{g0}(r_j^{(k)})] \qquad (19)$$

where Eq.(14) has been used to calculate $d[\ln(n_j/n_j^0)]/dt$ and the force experienced by each drop is

$$F_{drj} = m_{dj} \nu_{sj} \left(u_{srj} + \frac{1}{\rho_1} \frac{\partial p}{\partial r} \right) \qquad (20)$$

For each drop class j, in each of its rings, the drop size is determined by assuming that all such drops are identical and experience gas conditions at the edge of their sphere of influence (interstitial region denoted by subscript i) which are determined as averages over the ring radial interval and drop classes. If n_d is the average total drop density in the ring, the radius of a drop sphere of influence (Bellan and Harstad, 1988), R_i, is calculated from $4\pi R_i^3 n_d/3 = PF$ where the packing factor, $PF = 0.74$ (Bellan and Cuffel, 1983). For class j, the average gas temperature in its sphere of influence, T_{gi}, is related to the gas temperature at the edge, T_j, through an expansion in R_j/R_i of an expression derived in previous models (Bellan and Harstad, 1988)

$$T_{gi} = \tilde{\alpha}_j T_{gj} \qquad (21)$$

where $\tilde{\alpha}_j \sim 1 + 2\lambda_j + 7\lambda_j^2$ and $\lambda_j \equiv (1 - T_{gj}/T_g) R_j n_d^{1/3}$ with $\lambda_j c < 1$, and T_g is the average gas temperature over all classes at a given r_c. Similarly, $\rho_{gi} = \rho_{gj}/\tilde{\alpha}_j$, where ρ_g is the gas density, i refers to the interstitial space between drops and j to the initial size class. Averaging over the size classes,

$$T_{gi} = < \tilde{\alpha}_j > T_g \qquad (22)$$

where approximately, $<\tilde{\alpha}_j> = 1 + 2 < \lambda_j > + 4 < \lambda_j >^2 + 3 < \lambda_j^2 >$. Averaging is done using weights n_j/n_d.

Thus, the evaporation rate of class j, $\dot{m}_{dj}$, and R_j can be calculated using the previously derived model (Bellan and Harstad, 1988) of drop heating and evaporation in its own sphere of influence. The difference between the previous model and the present model is that here the circulation inside the drop is taken into account in the calculation of the drop

temperature using the effective-conduction correction proposed in Abramzon and Sirignano (1989) as it has already been done by Harstad and Bellan (1991). Accordingly, the Ranz-Marshall correlation is no longer used here. Instead, in the boundary condition at the drop surface, the gas conductivity coefficient is multiplied by the Nusselt number expression valid for laminar flow (the drop Reynolds number based upon c $\vec{u}_{si}$> is less than 102).

B. Conservation Equations for the Gas

The conservation equations for the gas are:

Mass conservation:

$$\partial \rho_g / \partial t + [\, \partial (r \rho_g \, u_{gr}) / \partial r] / r = - \sum_j n_j \, \dot{m}_{dj} \qquad (23)$$

Radial momentum conservation:

$$\rho_g \left(\frac{\partial u_{gr}}{\partial t} + u_{gr} \frac{\partial u_{gr}}{\partial r} - \frac{\bar{u}_{g\theta}^2}{r} \right) + \frac{\partial p}{\partial r} = F_{gr} \qquad (24)$$

where p is given by Eq.(1) and a null net gas - drops interaction for global radial momentum conservation requires that

$$F_{gr} = - \sum_j n_j \, (F_{drj} + \dot{m}_{dj} \, u_{srj}) \qquad (25)$$

$$F_{gr} = \sum_j n_j (\nu_{sj} \, m_{dj} - \dot{m}_{dj}) \, u_{srj} + \frac{1}{\rho_l} \left(\sum_j n_j \, m_{dj} \right) \frac{\partial \hat{p}}{\partial r} \qquad (26)$$

Since p' satisfies the Bernoulli relationship, it can be considered as an approximate quasi - steady solution to

$$\rho_g \left(\frac{\partial u_{gr}}{\partial t} + u_{gr} \frac{\partial u_{gr}}{\partial r} \right) + \frac{\partial p'}{\partial r} = 0 \qquad (27)$$

and $\tilde{p}$ is given by

$$\partial \tilde{p} / \partial r = \rho_g \, u_{g0}^2 / r \qquad (28)$$

The vortex develops quickly a core devoid of drops (Bellan and Harstad, 1988) and the contribution $\tilde{p}$ to the pressure might be important for small r because $u_{g0} \approx r^{-1}$ and the centrifugal force may be substantial for high vortex strength. The value $\tilde{p}=0$ is taken at the outer vortex edge, giving inside the cluster

$$\tilde{p} = - \int_r^{r_{max}} \rho_g \, \Gamma_{g0}^2 \, dr / r^3 . \qquad (29)$$

From Eq. (24) it can be concluded that the quasi-static gradient, $\partial \hat{p} / \partial r$, can be identified with the volume gas force. By defining the liquid volume fraction $f_{vl} \equiv (\sum n_j m_{dj}) / \rho_l$ and combining Eqs. (24), (27) and (28) one can calculate

$$F_{gr} = \frac{\partial \hat{p}}{\partial r} = \frac{\sum_j n_j (\nu_{sj} \, m_{dj} - \dot{m}_{dj}) \, u_{srj}}{(1 - f_{vl})} \qquad (30)$$

Eq. (30) shows that it is the volume force F_{gr} which describes the effect of cluster "porosity", As $f_{vl} \to 1$, the cluster acts as one large liquid drop and the pressure gradient $\partial \hat{p} / \partial r$ becomes unbounded unless $u_{sr} \to 0$.

Azimuthal momentum conservation:

$$\rho_g \left(\frac{\partial J_{g0}}{\partial t} + u_{gr} \frac{\partial u_{g0}}{\partial r} + \frac{1}{r} u_{gr} \, u_{g0} \right) = F_{g0} \qquad (31)$$

where

$$F_{g\theta} = \sum_j n_j (\nu_{sj} m_{dj} - \dot{m}_{dj}) u_{s\theta j} \tag{32}$$

Combining Eqs. (23) and (31) one obtains

$$\frac{\partial}{\partial t}(\rho_g u_{g\theta}) + \frac{1}{r^2}\frac{\partial}{\partial r}(r^2 \rho_g u_{gr} u_{g\theta}) = \tilde{F}_{g\theta} \tag{33}$$

where

$$\tilde{F}_{g\theta} \equiv F_{g\theta} - u_{g\theta}\sum_j \dot{m}_{dj} = \sum_j n_j (\nu_{sj} m_{dj} u_{s\theta j} - \dot{m}_{dj} u_{d\theta j}) \tag{34}$$

It is convenient now to define a cluster velocity UC such that

$$U_{cr}^k = \frac{dr_c^k}{dt} \tag{35}$$

and by definition

$$P_{g\theta}^{(k-1/2)} \equiv \int_{r_c^{k-1}}^{r_c^k} \rho_g \Gamma_{g\theta} r\, dr \tag{36}$$

Using Eqs.(14), (33), and (34) it is found that

$$^{*}dt P_{g\theta}^{k-1/2} \cdot \int_{r_c^{k-1}}^{r_c^k} \tilde{F}_{g\theta}\, r^2 dr + \Delta_k [r \rho_g \Gamma_{g\theta} (u_{cr} - u_{gr}) 1 \tag{37}$$

where Δ_k is an operator defined by

$$\Delta_k V \equiv V_k - V_{k-1} \tag{38}$$

What is now desired is a choice of u_{cr} such that the coordinate system associated with the cluster, r_c, follows all of the drops in the cluster. Such a coordinate system would not be obtained for values of u_{cr} such that the total angular momentum is a constant of motion because the largest initial size class drops would centrifuge beyond the cluster edge. For this reason ring-average gas mass and gas azimuthal momentum are defined as

$$M_g^{k-1/2} = \int_{r_c^{k-1}}^{r_c^k} \rho_g \, r \, dr \tag{39}$$

$$\bar{\Gamma}_{g0}^{k-1/2} = P_{g0}^{k-1/2} / M_g^{k-1/2} \tag{40}$$

where $\bar{\Gamma}_{g0}^{k-1/2} = r_c^{k-1/2} u_{g0}^{k-1/2}$. With these new notations Eqs. (23), (34) and (37) yield the following conservation equation for P_{g0}

$$M_g^{k-1/2} \frac{d}{dt} \bar{\Gamma}_{g0}^{k-1/2} = \int_{r_c^{k-1}}^{r_c^k} r \left[\sum_j n_j (v_{gj} m_{dj} - \dot{m}_{dj}) (\Gamma_{d0j} - \bar{\Gamma}_{g0}^{k-1/2}) \right] dr$$

$$+ \Delta_k \left[r \rho_g (u_{cr} - u_{gr}) (\Gamma_{g0} - \bar{\Gamma}_{g0}^{k-1/2}) \right] \tag{41}$$

where the choice has been made for u_{cr} to be

$$u_{cr} = \left(\sum_j n_j \, \ell_{dj} \, u_{drj} \right) / \left(\sum_j n_j \, \ell_j \right) \tag{42}$$

Note that in Eq.(41) the integral term gives the relaxation of angular momentum between the gas and drops, whereas the difference term represents a source at the ring boundaries. This source is null for irrotational (constant Γ_{g0}) flow.

Species conservation:

$$\partial(\rho_g Y_F)/\partial t + [\partial(r\rho_g u_{gr} Y_F)/\partial r]/r = -\sum_j n_j \dot{m}_{dj} + \frac{1}{r}\frac{\partial}{\partial r}\left[D_T \rho_g r \frac{\partial}{\partial r}(Y_F)\right] \quad (43)$$

where Y_F is the gas mass fraction of the evaporating liquid component averaged over drop spheres of influence. The value of D_T is calculated from the definition of the Schmidt number,

$$D_T = \frac{\mu_g + \mu_T}{\rho_g Sc_g} \quad (44)$$

where μ_T is given by Eq.(6) and Sc_g is prescribed.

Energy conservation:

$$\partial(\rho_g h_g)/\partial t + [\partial(r\rho_g u_{gr} h_g)/\partial r]/r = [\partial(rk_g \partial T_g/\partial r)/\partial r]/r$$

$$+ \sum_j n_j [\dot{m}_{dj}(\Delta h_{evap,j} - C_{pF} T_{gs,j} - 0.5 u_{sj}^2) + v_{sj} m_{dj} u_{sj}^2] \quad (45)$$

where $h_g = C_{pg} T_g$, $\rho_g h_g = \gamma p/(\gamma - 1)$ is the enthalpy, where y is the ratio of the heat capacities, C_p is the specific heat capacity at constant pressure, k is the conductivity, T_{gs} is the drop surface temperature and Δh_{evap} is the heat transferred to the drop from the gas per unit mass of evaporated fuel. The third term in the right hand side of Eq. (45) represents the change in the thermal energy of the gas due to incoming fuel vapor, the fourth term represents the change in the kinetic energy of the gas due to incoming fuel vapor and the last term represents viscous dissipation from drag.

The value of k_g is calculated from the definition of the Prandtl number

$$k_g = \frac{(\mu_g + \mu_T) C_p}{PI_g} \qquad (46)$$

where μ_T is given by Eq.(6) and Pr_g is prescribed. It is assumed that the Lewis number of the gas is unity, and thus that $Sc_g = Pr_g$.

Equation of state:

The ideal gas law is used to relate the pressure, temperature, density and mass fractions. Since the ambient pressure is assumed constant and the other pressure contributions are small, and since C_{pg} is constant, this means that approximately $\partial(\rho_g h_g)/\partial t = O$. Thus Eq.(45) becomes quasi-steady and determines u_{gr}.

4. METHOD OF SOLUTION

Let JT be the total number of initial size classes; thus there are JT + 1 coordinate systems previously defined. Each initial size class has its own system of coordinates, and the gas in the cluster has a coordinate system of its own.

The conservation equations in general are solved in Lagrangian frames, whereas the gas energy equation is solved in an Eulerian frame as a radial difference equation.

To solve the gas conservation equations, equations (23) and (43) are integrated over intervals in r_c by evaluating the non-exactly-integrable term at $r_c^{(k+1/2)}$ according to the definition of Eq. (10). This yields equations for the time evolution of average gas and liquid vapor niasses in the corresponding rings. Equation (45) is integrated in the same way with the difference that it is steady because Mach $<<$ 1.

The value of p_{amb} is known and $\tilde{p}$ is calculated using Eq. (29), p' is calculated from

Bernouilli's relation, Eq.(2), and $\hat{p}$ from Eq.(30). The gas energy equation determines $u_{gr}(t,r)$ and hence $u_s(t,r)$, while $T_g(t,r)$ is calculated from the equation of state, knowing p. Further, $\rho_g(t,r)$ and $Y_F(t,r)$ are calculated from ring versions of Eqs. (23) and (43) respectively; the values of Γ_{g0} determine u_{g0}; r_j and constants N_j determine n_j; Γ_{d0j} is calculated from Eq.(19); r_j and u_{drj} are calculated from Eqs. (17) and (18) respectively; and the drops characteristics are calculated using previously developed models (Bellan and Harstad, 1988; Harstad and Bellan, 1991).

The system of equations is solved as a large set of first order differential equations using piecewise linear interpolation procedures between the r_c and r_j coordinates. These interpolations allow the calculation of the dropdependent variables in the system of coordinates of the gas.

5. INITIAL CONDITIONS

Appendix I shows that one cannot chose an arbitrary initial distribution for u_{d0}, $u_{d0}^{\circ}(r^{\circ})$, because the Jacobian, J, of the mapping $r^{\circ} \rightarrow r$ may become null and the system of equations for the drops becomes singular. A sufficient condition for the mapping to be regular, is that the Jacobian be quasi-steady. This imposes a constraint on $u_{d\theta}^{\circ}(r^{\circ})$ as follows.

If $u_{dr}^{\circ} = O$, then $(dJ/dt)^{\circ} = O$. Additionally, $(d^2J/dt^2)^{\circ} = O$ if $(du_{dr}/dt)^{\circ} = A^{\circ}$, where A° is constant. Therefore $u_{d\theta}^{\circ}(r^{\circ})$ is determined through the momentum equation as

$$\left(\frac{u_{d\theta}^2}{r}\right)^{0} = A^{\circ} - v_s^{\circ} u_{gr}^{\circ} \tag{47}$$

$$u_{d\theta}^{\circ} = \sqrt{r^{\circ}[A^{\circ} - v_s^{\circ}\, u_{gr}^{\circ}(r^{\circ})]} \tag{48}$$

with A“ ≥ v,” max (uV”).

Note that since $u_{d\theta}$ eventually relaxes to $u_{g\theta}$, it is still possible to generate a singularity at long times for certain choices of $u_{g\theta}°(r°)$. However, the use of turbulent diffusion mitigates the effect and a singularity can be avoided,

Thus, for each initial size class, the initial drop radial acceleration and initial drop azimuthal velocity are prescribed as above. The initial drop azimuthal velocity may contain an additional term with respect to the expression in Eq.(48). This is a drop cluster solid body rotation, $B_{d\theta}°$, which leads to additional cluster expansion, Furthermore, the initial drop size of each initial size class. and the initial drop temperature are prescribed as well.

The initial drop number density for each initial size class j is defined from the total number of drops per length of vortex, N_j^t, and the radial distribution of the probability of finding a drop from class j at location r, $\varrho_j(r)$, as follows

$$n, = N_j^t \varrho_j\ (r)\ for\ r_{in} \le r \le r_{out} \qquad (49)$$

$$N_j^t = 2\pi \int_0^\infty n_j r dr \qquad (50)$$

where r_{in} is the inner boundary and r_{out} is the outer boundary of the cluster.

Function ϱ_j (r) can be measured in a practical setting . In absence of such data, ϱ_j (r) can be chosen arbitrarily and considered as a parameter of the problem. For a given, fixed, number $O < q_j < \infty$, ϱ_j (r) is chosen here

$$\varrho_j\ (r) = A_{q_j}\ \eta^{q_j}\ e^{-q_j \eta} \qquad (51)$$

where

$$\eta \equiv (r - r_{in})/r_{q_j}\ ,\ thus\ 0 \le \eta \le \eta_{out} \qquad \textbf{(52a)}$$

$$\max\ \varrho_j(r) = A_{q_j}\, e^{-q_j} \quad at\ \eta = 1 \qquad \textbf{(52b)}$$

with

$$r_{in,\,j} \equiv b_{ij}\ R_c^o\ ,\quad 0 \le b_{ij} \le 1 \qquad (53a)$$

$$r_{out,j} = b_{0j}\ R_c^o\ ,\ b_{ij} < b_{0j} \le 1 \qquad \textbf{(53b)}$$

$$r_{q_j} \equiv \alpha_j\,(r_{out,\,j} - r_{in,\,j})\ ,\quad 0 \le \alpha_j \le 1 \qquad \textbf{(53c)}$$

Note that $\eta_{out,\,j} = \alpha_j^{-1}$, and the maximum value of n_j is located at a fraction α_j of distance from the inner edge ring to the outer edge. If $q_j \to 0$, then the distribution is uniform; if $q_j >> 1$, the distribution assumes a sharp, Dirac delta function distribution. The value of A_{qj} is found by requiring that

$$2\pi \int_{r_{in}}^{r_{out}} \varrho_j(r)\, r\, dr = 1 \qquad (54)$$

his results in

$$A_{q_j} = \left\{ 2\pi r_{q_j} \left[\frac{r_{in_j}}{q_j^{q_j+1}}\, \Upsilon\left(q_j+1, \frac{q_j}{\alpha_j}\right) + \frac{r_{q_j}}{q_j^{q_j+2}}\, \gamma\left(q_j+2, \frac{q_j}{\alpha_j}\right) \right]_{11}^{-1} \right. \qquad (55)$$

where

$$\gamma(a, b) \equiv \int_0^b t^{a-1} e^{-t} dt \qquad (56)$$

Function ρ_j (r) provides the spatial dependence of the drop number distribution, whereas N_j' can be prescribed, or max (n_j) can be prescribed, or the air/liquid mass ratio can be prescribed to yield an initial drop count,

Additional dependent variables which are prescribed are the initial gas pressure and temperature, the initial cluster radius, the initial irrotational component and the initial solid body rotation component of the gas tangential velocity.

The initial properties of gas (air) and liquid are prescribed as well. Constants A_T in Eq.(6) and C_t in Eq.(9) are considered parameters of the problem.

6. RESULTS

6.1 Typical behavior.

Due to the large number of parameters entering the above model, it was first deemed necessary to establish a baseline behavior. The guideline for what represents a baseline situation was obtained from previous models and results (Bellan and Harstad, 1990) describing the behavior of monodisperse, uniformly distributed clusters of drops in vertical flows. The results indicated that very dense sprays have a ratio of the radius of the sphere of influence (Bellan and Cuffel, 1983) by the drop radius which is 10 or less. For dense sprays this ratio is between 10 and 15, whereas for moderately dense sprays this ratio varies between 15 and 30. Dilute sprays are those for which this ratio is larger than 30. For example, when the liquid is n-decane it was found that for an air/liquid mass ratio of 0.314 (stoichiometric is 15.7) the cluster was dense, whereas for a mass ratio of 0.785 the cluster

was moderately dense (Bellan and Harstad, 1990). An air/liquid mass ratio of 1.57 was found to be on the borderline between the moderately dense and dilute regimes (Bellan and Harstad, 1990).

In the present mode.], the drop number density is no longer required to be uniform, and the initial drop size is no longer monodispcrse, so that, depending on the curve shape of th e initial drop number distribution, a global air/liquid mass ratio of 0.314 might create regions having very dense, moderately dense and dilute characteristics.

For the choice of parameters α_j and q_j in the distribution function, the plots in Fig. 3 show that the initial distribution is mostly dense, except for the inner part of the cluster, thus making comparisons with previous results more meaningful. It should be realized though that because the ratio plotted is an average, within their own initial size class the drops might be in a denser or more dilute configuration depending on the parameter which specifies $\max(n^o_j)$ for each initial size class. Plots of the characteristic ratio discussed above are shown in Figs. 4a and 4b for the two initial size classes considered in this baseline situation.

The total drop number density is illustrated in Fig. 5a versus the gas radial coordinate. The initial profile evolves into an increasing function of the radial coordinate except for the outer boundary region of the cluster. The innermost region of the cluster devoid of drops becomes larger as they are centrifuged to the outer portions of the vortex. In this region the population is initially dominated by the initially smaller drops and remains composed mostly of the initially smaller drops (initial-size-class-1) as shown in Figs. 5b and SC. Although at the outer edge initial-size-class-1 drops are initially more populous, as the calculation proceeds and the cluster expands, initial-size-class-2 drops which are initially larger are

centrifuged further out. Since their evaporation rat e is slower (because their heating time is larger), they continue to stay larger and thus be centrifuged further. The central part of the vortex is initially dominated and continues to be composed of initial-size- class-1 drops,

Evidence of the distribution of the two initial size classes within the cluster, as well as information regarding the drops sizes at different times can be found in Fig. 6. The plots show that each initial size class develops a size distribution of its own according to the location of the drops within the cluster. Drops at the cluster periphery evaporate faster because they are in contact with hotter gas (see Fig. 7), whereas drops located near the mean cluster radius evaporate slower because the gas temperature is lower (see Fig. 7). The lower gas temperature in this part of the cluster is attributed to the initially higher drop number density. A larger number of drops represents a larger heat sink for the gas, as the drops heat up (due to the. temperature difference) and the liquid evaporates. The larger gas temperature at the outer cluster periphery is due to the continuous supply of hot gas from the surroundings of the cluster, as the cluster expands into the hotter surroundings. The larger gas temperature at the inner cluster periphery results from the depletion of drops by centrif ugati on. In the absence of drops there is no heat sink on the gas, and the temperature stays close to its initial value. A sharp temperature gradient develops as r_c increases, corresponding to the increase in the drop number density. The nonmonotonic behavior for $r_c <$ lcm is attributed to different contributions to the drop number density from the two initial size classes. The total drop number density is a monotonically increasing function of r_c within the mean region of the cluster, however, the drop number density for initial-size-class-2 evolves into a profile exhibiting a slight minimum within the mean region

of the cluster. This slight minimum corresponds to the slight local maximum in the temperature profile since there is a decreasing heat sink on the gas. This slight local temperature maximum impacts evaporation and the plots on Fig. 6b show the evolution of a slight dip in the curve occurring for r_c slightly smaller than 1 cm.

The evolution of the drop number density profiles is elucidated by examining the evolution of the drop tangential velocities and that of the angle of the velocity vector with the tangential coordinate. The tangential velocities exhibit a minimum at a location close to the inner cluster periphery whereas the velocity angle exhibits a maximum at the same location; this maximum decreases with time and shifts towards larger values of r_c. The minimum tangential velocity is responsible for the accumulation of drops and for the resulting sharp increase in the drop number density close to the inner cluster periphery. The velocity angle reflects both tangential motion as well as centrifugation of particles; as time increases, the largest centrifugation shifts from the inner cluster periphery to the central region of the vortex.

Figure 8 illustrates the development of the mass fraction profile of the evaporated liquid, Y_F. For small times the profile is asymmetric with respect to the mean radial location in the cluster. The smaller mass fraction of evaporated liquid, both at the inner and outer cluster periphery, corresponds to regions of low drop number density. For large times, the profiles become almost symmetric with respect to the mean radial location in the cluster and the mean evolves almost into a plateau. The low Y_F values at the inner and outer cluster peripheries still correspond to the regions of low drop number density. The sharp edge developed between the inner cluster periphery and the mean plateau corresponds to the

sharp edge in the drop number density at the same location.

6.2 Effect of the initial air/liquid mass ratio.

Results from calculations performed with initial air/liquid mass ratio, Φ°, of 0.785 and 0.157 are. compared with those obtained with $\Phi^\circ = 0.314$ in Figs. 9-14. All other values of initial conditions and parameters remain the same (see Fig. 3 caption).

A comparison between the ratio of the average drop radius and the radius of the sphere of influence is shown in Fig. 9 as an indication of the denseness of the cluster. Denser clusters contain more mass and thus the centrifugal force is larger. As a consequence, the drops are centrifuged further out when the spray is denser, as clearly shown in Fig. 10 where the total drop number density is depicted versus the gas coordinate in the cluster for the three different calculations at the same times. It is interesting to notice that as the cluster is chosen initially more dilute, the drop number density becomes more uniform inside the cluster with the exception of the inner and outer peripheries of the cluster. This is related to the change in the drop velocities profiles. As shown in Fig. 11a, in a more dilute cluster the drop radial velocity is larger in the inner part than in the outer part; the opposite occurs in a denser cluster. Figure 11b shows a similar change in behavior for the drop tangential velocity with an additional development of a more uniform profile in the central and outer part of the cluster. The structure of the velocity profile is tightly coupled to the drop number density through the drag force and the evaporation rate, and thus a direct cause and effect explanation is not possible. The results illustrated in Fig. 10 give support to the assumption of uniformity of the drop number distribution for dilute clusters of drops. For dense clusters of drops the assumption does not appear to be realistic.

Portrayed in Fig. 12 is the gas temperature profile at three selected times versus the radial coordinate for the three air/liquid mass ratios. When the initial drop temperature is lower than that of the gas, a denser cluster of drops represents a greater heat sink on the gas, resulting in considerable lower temperatures in the center of the cluster.

The result of the interaction between drops ancl gas is also clearly seen in Fig. 13 where the residual drop radius (ratio of drop radius by the initial drop radius) is plotted versus the radial coordinate for both initial size classes at various times. The drops in denser clusters take considerably longer to evaporate and the drop size distribution is substantially more nonuniform. This is because the drop competition for heat results in a slower heating rate, and the heat transported from the cluster boundaries towards the interior has greater difficulty reaching the central part of the cluster. The results plotted in Fig. 13 show that the situation is exacerbated for the initially larger chops.

The distribution of the mass fraction of the evaporated component, Y_F, is the result of both the drop number density distribution and the evaporation rate, Figure 14 shows that as the cluster is initially denser not only is the maximum value of Y_F larger but the distribution is more symmetric with respect to the mean location in the cluster. The last effect is attributed to the greater centrifugation which (differentially) brings drops to the outer cluster boundary.

6.3 Influence of the initial drop size distribution at fixed air/liquid mass ratio.

The simplest initial drop size distribution is the monodisperse one. Thus, calculations were performed for $\Phi^o = 0.314$ with $R^o = 2 \times 10^{-3}$ cm. Although the inverse of the nondimensional radius of the sphere of influence is exactly the same as in the typical

calculations described in 6.1, the drop number density is much larger (see Fig. 15) than in the bimodal initial distribution of the baseline calculation because the liquid mass is the same but a substantial number of drops is smaller. Since the drops are on average smaller, centrifugation effects are reduced with respect to the typical calculation, which means that the drops penetrate less into the hot ambient. Thus, the gas temperature distribution is almost identical to that of the baseline calculation, except for the outer third of the cluster where it is substantially lower. For the drops located in the outer half of the cluster this results in a slightly reduced evaporation rate towards the end of the drop lifetime. Thus, it is the air/liquid mass ratio which controls dynamics and evaporation in the inner half of the cluster, whereas it is the drop size distribution which controls dynamics and evaporation in the outer half of the cluster. It is remarkable to notice the strong, persisting nonuniformity in the drop number density and the quickly-evolving nonuniformity in the drop size distribution during the early part of the calculation in the inner part of the cluster. For example, when t = 3.57×10^{3} sec the residual drop size at the inner cluster boundary, located at located at $r_c = 0.12$cm, is 5×10^{-2} whereas at $r_c = 0.8$cm the residual drop size is 5.2×10^{-1}.

An interesting theoretical question is what happens to an initially uniform drop number density and mono disperse size distribution. Calculations were performed for a monodisperse distribution with $R^o = 2 \times 10^{3}$ cm and $\Phi^o = 0.314$ for an initially uniform drop number density (q = 103). The results show that except for the outer and inner portions of the cluster (20% and 10% of the radial span respectively), the drop number density distribution remains uniform. However, neither the gas temperature distribution, nor the residual drop

radius stay uniform because even if the distribution of drops is uniform, the heat transfer characteristic time is larger than the drop lifetime. Thus the drops at the cluster periphery act as a "screen" for heat, and only that amount of heat which is not used by the drops at the edges of the cluster can penetrate to the central region of the cluster. In the central region of the cluster the gas temperature is considerably lower than at the periphery because a large amount of heat. is extracted by the drops from the gas (due to the temperature difference) and does not get replenished. For example, when $t = 3.565 \times 10^{3}$ see, the maximum residual drop size is 0.52, whereas the drops at the inner edge of the cluster have completely evaporated and the residual size of the drops at the outer cluster edge is 0.31. Comparing thus these results with the study of Bellan and Harstad (1990), it is concluded that if the initial drop number density distribution is uniform, it can be assumed that it will stay uniform in most of the cluster, whereas if the initial drop size distribution is uniform, it cannot be assumed that it would remain uniform.

The effect of changing one of the initial drop sizes in a bimodal distribution was investigated both for $\Phi^{o} = 0.314$ and $\Phi^{o} = 0.785$. In both cases the initial-size-class-2 was taken to have $R_2^{o} = 3.0 \times 10^{-3}$ cm instead of $R_2^{o} = 2.5 \times 10^{3}$ cm. When R_2^{o} is larger, the initial drop number density is lower (because the initial total mass is the same), and centrifugation effects are expected to become eventually more important. However, since when $\Phi^{o} = 0.785$ there is less liquid mass than when $\Phi^{o} = 0.314$, centrifugation effects play a less important role. The two drop number distributions in Fig. 16 should be compared with those of Fig. 5a (compared to 16a) and of Fig. 10 (middle graph to be compared to 16b). In Fig. 16a, the finite number of drops still present at the outer cluster periphery at

the end of the calculation belong to initial-size-class-2 as these larger drops have not completely evaporated when the calculation was terminated (as can be seen in Fig. 17 b). Since the initial ratio of maximum drop number density was kept the same as in the previous calculations, the drop number density of initial-size-class-1 is now smaller than in the baseline calculation. This is why the drops in initial-size-class-1 evaporate at approximately the same rate as in the typical run, while being centrifuged slightly more. A small increase in the evaporation rate of the drops in the outer half of the cluster (see Fig. 17a and 6a) is attributed to the fact that initial-size-class-2 eventually expands the cluster further out and allows more heat to penetrate the cluster. This is easily seen in Fig. 18 where it is noticed that the gas temperature is eventually substantially higher at the edge of the cluster when initial-size-class-2 consists of larger drops, At early times, the larger value of n when R_2^o is smaller promotes a stronger interaction between drops and gas. As the drops are centrifuged, they take the gas along with them, and this increases u_{gr}. Therefore, the cluster expands more into the ambient encountering larger gas temperatures and thus promoting heat transfer. The result is a larger gas temperature at the outer edge of the cluster, as shown on Fig. *18.*

The centrifugation of these larger drops is also an effective mechanism for dispersing vapor into the ambient, as illustrated in Fig. 19, When comparing the plots of Fig. 19 with those of Fig. 8 it can be seen that although the maximum mass fraction of the evaporated compound is slightly lower when the drops in initial-size-class-2 are larger, vapor penetration into the ambient is more effective. This physical picture is in agreement with the well established fact in spray combustion that the small drops in a spray are responsible for spray

ignition, whereas it is the fuel vapor produced by the larger drops which is responsible for flame propagation.

All these effects are greatly reduced when $\Phi^o = 0.785$ instead of $\Phi^o = 0.314$. This indicates that the dense regions of a spray contain more control parameters than the dilute regions of a spray. Thus, any spray optimization process will have greater chance of success if it is initiated near the atomizer, in the dense spray region.

Since for a given Φ^o, at a fixed time, a larger maximum vapor mass fraction is obtained when initial-size-class-2 has a smaller drop size, whereas a larger vapor penetration into the ambient is obtained when the initial-size-class-2 has a larger drop size, the question arises as to whether a trimodal distribution evolves in a manner that combines both (desirable) characteristics (from the point of view of combustion of atomized liquid fuel). Figures 20-2,3 illustrate results obtained with a trimodal distribution when $R^o_1 = 2 \times 10^{-3}$ cm, $R^o_2 = 2.5 \times$ 10-3 cm and $R^0_3 = 3 \times 103$ cm where the maximum drop number density of the third initial size class was chosen to be one half of the second initial size class, while $\Phi^o = 0.314$. Plots of the evolution of the total drop number distribution and the three drop number distributions are found in Fig. 20, whereas plots of the gas temperature and vapor mass fraction appear in Figs. 21 and 22 respectively. For comparison, the residual drop radius for all three initial size classes appear in Fig. 23. These figures show that because of both differential centrifugation and differential evaporation according to the initial size class, the cluster penetrates more into the ambient when compared with the bimodal distributions where $R^o_2 = 2.5 \times 10^{-3}$ cm, and the maximum vapor mass fraction is larger than when $R^o_2 = 3 \times 10^{-3}$ cm. It is also interesting to notice that the gas temperature at the outer cluster

edge is almost as high as when $R^{\circ}_2 = 3.0 \times 10^{-3}$ cm, whereas the gas temperature close to the inner cluster edge, at the innermost radial coordinate where all size classes coexist, is lower than in either bimodal distributions calculations because of the higher total drop number density. Except at this particular location, the drops from initial-size-class-1 evaporate at the same rate as in the bimodal distributions where $R^{\circ}_2 = 3.0 \times 10^{-3}$ cm, however, their initial drop number density is slightly lower. The introduction of the third initial drop size has a much larger impact on the drop number density of the second initial size class, lowering it by about 20%. This results in a smaller centrifugation of this initial size class and thus a slightly slower evaporation rate towards the outer cluster edge. A lower evaporation rate can also be observed towards the inner cluster edge, and this is attributed to the lower gas temperature at that location, as explained above. The evaporation rate of the third initial size class is considerably lower in the neighborhood of both the inner and outer boundaries than it was on the bimodal size distribution, despite an initial drop number density which is less than one half than in that calculation. The larger drop sizes enhance centrifugation of this size class, particularly at the inner cluster boundary.

The conclusions from the above discussion is that polydispersity enhances penetration of the evaporated compound into the ambient as well as increases the maximum of the mass fraction of the evaporated compound within the cluster. Thus, polydispersity is recommended in the context of spray combusti on.

Since it has been established that polydispersity is beneficial in spray combustion, it is worthwhile exploring whether the relative number of drops in the initial size distribution has an important impact on the quantity and distribution of the evaporated compound. Thus,

calculations were performed for the same conditions as in the baseline situation except that the maximum drop number density was switched between the two initial size classes. The result is a lower total drop number density (by about 25%) since more mass is contained in the initially larger-size class drops which now has a much larger drop number density. Comparisons of the results of this calculation with those of the baseline case show that centrifugal effects are dependent upon the drop number density. For the same mass, a smaller drop number density results in a smaller centrifugation. Comparisons between early time behavior in Figs. 8 and 24 show that the evaporation rate is now slower and the evaporated compound does not penetrate as much as before into the ambient, Thus, for the purpose of spray combustion it is recommended that a polydisperse distribution should contain a proportionally larger number of small drops than of the larger drops.

6.4 Effect of the initial temperature difference between drops and gas.

In order to investigate the effect of the temperature difference between drops and gas, the initial temperature of the drops was lowered by 50K to 300K. Thus, it is expected that the heat up time of the drops will become relatively more important and that the lifetime of the drops will increase. As the drops require more heat, the gas temperature decreases to a greater extent; this is illustrated in Fig. 25. As the drops survive longer, centrifugal forces have a longer time to act resulting in greater penetration into the ambient. The plots in Fig. 26 show that when the calculation is ended, the drops located in the central part of the cluster and belonging to initial-size-class-2 have not evaporated and their size is up to 60% of the initial one. However, since their drop number density is rather low (about 2 x $10^3 cm^{-3}$), the amount of mass left to evaporate is small.

Examination of the gas temperature profile together with the evaporated mass fraction profile (Figure 27) reveals that in the context of spray combustion, if ignition has not been initiated before 2.866×10^{-3} see, then any possible ignition would occur at the outer edge of the cluster where both the gas temperature is maximum and the fuel mass fraction is high (although not maximum; the maximum Y_F occurs at a location where the gas temperature is considerably lower).

Thus, increasing the temperature difference between gas and drops by decreasing the drop temperature results in additional nonuniformities in the cluster, as well as a delay in evaporation which allows increasing drop centrifugation and therefore penetration of the vapor into the ambient.

6.5 Effect of the normal boiling temperature.

In all calculations above, the liquid was chosen to be n-decane and the value of the thermophysical properties used is listed in Table I. In order to study the importance of the normal boiling point temperature, its value was increased from 447.7K to 800K, thus creating an artificial liquid with the properties of n-decane except for the normal boiling point temperature.

The results obtained with these new conditions show that even for moderately dense clusters ($\Phi^o = 0.785$), a higher normal boiling point temperature will represent a considerable heat sink for the gas, and thus enhance nonuniformities in drop size throughout the cluster. Drops located in the outer part of the cluster evaporate considerably faster resulting in a monotonically increasing profile for Y_F starting from the cluster inner boundary. Evaporation is considerably delayed, especially in the central part of the cluster which

become quickly depleted ofheat.

6.6 Effect of the latent heat of evaporation.

The same strategy as above was used to study the influence of the latent heat of evaporation: the latent heat of evaporation was artificially increased from 73.92 cal/g (the n-decane value) to 200 cal/g. Calculations were performed for $\Phi^o = 0.314$ with the bimodal initial size distribution of the baseline case. The results show again that evaporation is considerably delayed, particularly in the central part of the cluster where heat is being rapidly depleted. This heat cannot be replenished at a comparable rate because the incoming heat (from the ambient) is used by the drops at the cluster outer periphery to increase their temperature. The evaporation delay allows an increase in centrifugation and further penetration of the drops into the ambient, The resulting mass fraction profile of the evaporated component resembles that of the baseline case except that it is more nonuniform and has lower values.

6.7 Effect of the initial tangential gas velocity.

In order to explore the influence of the initial gas velocities upon the cluster, calculations were performed, with individual changes in the initial solid body rotation, B^o_{g0}, and the initial irrotational motion, A^o_{g0}, for the parameters listed in the Fig. 3 caption.

When B^o_{g0} is taken to be 200 see-l instead of being null, the initial gas tangential velocity increases considerably except at the inner cluster periphery. As a result, centrifugal effects are larger and the cluster expands more. Since transport processes are slower than expansion, the inner part of the cluster is marginally affected, whereas the outer cluster periphery is substantially affected. The effective result is that when B^o_{g0} = 200 see-l the

drops evaporate marginally faster inthe innerpart of the cluster, and substantially slower in the outer part of the cluster. The reason for the slower evaporation in the outer part of the cluster is the smaller slip velocity between drops and gas in that region. The increased centrifugation and resulting increased expansion into the hot environment cannot compensate for the reduction in the slip velocity.

An opposite behavior is encountered when increasing the initial drop irrotational motion, A°_{g0}, by a factor of 2 while keeping B°_{g0} = 200 see-l. When A°_{g0} is increased, the tangential gas velocity in the outer part of the cluster is only marginally affected, whereas the tangential gas velocity in the inner part of the cluster is considerably increased. Thus, centrifugation of the cluster into the ambient remains the same, however the vortex core region devoid of drops is enlarged. The increase of the slip velocity in the inner part of the cluster results in a higher evaporation rate and quicker drop disappearance.

The above discussion thus reveals drivers which control evaporation and dynamics of different parts of the cluster. The behavior of the outer part of the cluster is controlled by the solid body rotation of the gas, whereas the behavior of the inner part of the cluster is controlled by the irrotational motion of the gas. Examination of the drop number density distributions for each initial size class versus the radial coordinate corroborates this conclusion. Comparisons made at identical times show that when B°_{g0} is larger, the inner part of the distribution is very slightly affected whereas the outer part of the distribution shows lower values of n_i and a more spread-out distribution (towards the ambient). In contrast, when A°_{g0} increases, the outer part of the drop number density distribution remains identical whereas the inner part is substantially higher and the cluster inner radius is

substantially larger. Figure 28 illustrates profiles of the drop number density and the residual radius for initial-size-class-1 when A°_{g0} is respectively 100 cm^2/sec and 200 cm^2/see, for B°_{g0} = 200 see-l. By comparing the plots of Fig. 28c with those of Fig. 6a, one can clearly see the influence of B°_{g0}.

The compression of the shell of drops (which is in fact the cluster) with increasing A°_{g0} has been previously discussed in Bellan and Harstad (1990) for monodisperse, uniformly distributed clusters of drops. In the same publication, B°_{g0} was identified as an important parameter in determining the centrifugation of the drops. The novelty of the present results is to show that not only the size of the cluster is being affected by these parameters, but the profile of the drop number density distribution as well as that of the residual drop size distribution are affected as well.

6.8 Effect of the initial solid body rotation of the drops as an entity.

In Bellan and Harstad 1990, the initial solid body rotation of the drops as an entity was identi fied as an important parameter controlling both cluster dynamics and drop evaporation in the dense regime. Since that calculation was performed for monodisperse, uniformly distributed drops, it is interesting to investigate the influence of the same parameter in the present, more realistic, model. Thus, calculations were performed with $B^{\circ}_{d\theta}$ = 150 sec^{-1} and they were compared with the reference calculation where $B^{\circ}_{d\theta}$ = O see"*.

The results reveal that $B^{\circ}_{d\theta}$ controls the dynamics and thermodynamics of the cluster in a manner similar to B°_{g0}. The larger $u_{d\theta}$ increases the centrifugal force, and thus u_{dr} increases as well. Through momentum transfer to the gas, both u_{gr} and $u_{g\theta}$ increase as well. Because the characteristic time for momentum transfer is of same order of magnitude as the

evaporation time, the slip velocities between drops and gas are now larger, resulting in enhanced drop evaporation. All these effects become stronger as r increases due to the fact that B°_{d0} is multiplied by r in the initial prescription of the drop velocities.

The enhanced centrifugal motion disperses the drops further into the ambient and results in a larger engulfment. of the ambient hot gas. This explains the larger overall gas temperature within the cluster, especially at the outer cluster edge. The further penetration of the drops into the ambient (by more than 40% comparing to the reference case) is accompanied by a decrease in the local drop number density because the same number of drops occupy now a larger volume. However, at the outer cluster periphery (which is at different radial location here than in the reference case), the drop number density is the same. This density apparently reflects the value necessary for turbulent diffusion and porosity pressure $\hat{p}$ to prevent ring collapse (see Appendix I).

7'bus, the initial drop solid body rotation controls the drop number density and size of the drops, as well as the gas temperature within the cluster.

6.9 Effect of the initial cluster size

The initial cluster size was vaned in the calculations by independently varying the outer and inner initial cluster radius. Thus, the outer radius was increased by 5096 to 3 cm while keeping R°_{in} = 0.2 cm, and in another calculation the inner radius was decreased by 50% to 0.1 cm while keeping R°_{c} = 2 cm. Because in the present calculations the drop and gas velocities are initially prescribed as a function of the radial distance, it is difficult to uncouple from the results the unique effects of the cluster size. Therefore, all discussions below must be interpreted in the context of the change of other initial conditions associated with the

change in the cluster size.

Increasing the outer cluster radius while prescribing a self-similar (compared to the reference case) drop number distribution means that there are now more drops inside the cluster. Due to the dependence of the initial velocities upon r, the prescribed drop and gas velocities have now a much larger solid body component at the outer edge of the cluster. The much larger tangential drop velocity at the outer edge of the cluster induces a larger centrifugal force at that location, and thus a higher u_{dr} resulting in increasing expansion into the ambient, As the cluster expands into the ambient, it engulfs hot gas, but in contrast to the situation in 6.8 when this resulted in a larger gas temperature, here there is a larger number of drops inside the cluster which act as a heat sink, thereby resulting in a lower temperature at the outer cluster edge when compared to the reference case. The increased slip velocity at the outer cluster edge counterbalances the lower temperature at that location and enhances evaporation of the drops in both initial size classes. The increased slip velocity is also responsible for the increased fluxes of gas and evaporated species toward the inner part to the cluster. As an increased amount of gas is transferred to the inner part of the cluster, the tangential velocities of both drop and gas decrease, thus slightly decreasing the centrifugation of the inner-cluster-edge drops. This explains why the vortex core devoid of drops is now slightly smaller. The drag effect on the drops is to differentially decrease u_d more than u_g, resulting in a smaller slip velocity at the inner cluster edge. This in turn affects evaporation, and thus the residual drop size is now larger at that location.

When increasing the size of the cluster by decreasing the initial inner radius, the cluster contains an additional number of drops. At the inner cluster edge the gas is endowed with

a very large initial irrotational motion which is gradually transferred to the drops through momentum exchange. Since irrotational motion centrifuges while packing the particles, it is not surprising to see that the results show a maximum in the total, as well as in the initial classes, drop number distribution developing at the inner edge of the cluster (see Fig. 29). Thus, whereas in the reference case discussed in 6.1 the drop number densities were increasing functions of r, here the drop number densities are concave curves, with a maximum at the inner edge and an almost flat plateau in the central part of the cluster. The outer drop number distribution remains unchanged.

This new inner-edge drop-number-density maximum affects the gas temperature which is now substantially smaller at that location due to the heat sink represented by the increased number of drops per volume. This also results in larger residual drop radii (i.e. slower evaporation rate) at the inner edge of the cluster, while the remaining drops in the cluster are unaffected. Despite the slower local evaporation rate, the local mass fraction of the evaporated compound is larger due to the much larger drop number density.

The increased centrifugation of the inner edge drops results in a considerably larger vortex core devoid of drops. Since the centrifugation of the outer edge drops remains unchanged, the result is a smaller cluster volume even though the initial cluster volume was larger. Thus these limited results suggest that the ratio of the final cluster volume by the initial cluster volume is an increasing function of R^{o}_{in} under the present assumptions.

"For the type of initial conditions chosen in this model, the results show that the dependent variables are not self-similar when the initial size of the cluster is varied, The results also show that the behavior of the cluster is different if the volume is increased by

decreasing R^{o}_{in} or by increasing $R^{"}_{c}$. This is because the inner part of the vortex is dominated by irrotational motion, whereas the outer part of the vortex is dominated by solid body rotation. Irrotational motion centrifuges and packs the particles as, seen in Fig. 29, whereas solid body rotation centrifuges the particles and pulls the cluster apart by dispersing the particles as discussed in *6.8*.

6.10 Effect of transport from ambient to the cluster

It has already been mentioned in 2. that heat (and mass) transfer between the cluster to the ambient are modeled only globally through the use of a Nusselt number whose expression is given by Eq.(9). Constant C_1 appearing in that expansion has been estimated to have a typical value of 0.35, but it is obviously of interest to investigate the cluster behavior for departures from this estimated value. This is why calculations were performed for the parameters of the typical run, except that C_1 = 0.175. This smaller value of C_1 reduces heat and mass transfer to the cluster resulting in lower gas temperatures in the outer third part of the cluster. At the outer cluster edge, the gas temperature is now 10% lower than in the typical situation. This lower gas temperature has the effect of reducing the evaporation rate, resulting now in slightly larger drops towards the outer cluster boundary. Although the evaporation rate is now lower in that region, the mass fraction of the evaporated compound is now larger (by about 20% at the cluster outer edge) because there is less air entering the cluster from the ambient. Because the mass fraction of the evaporated compound is now larger, the corresponding flux and the flux of gas towards the vortex core are larger as well. All these changes affect only the outer third of the cluster, with no changes occurring in the remaining part of the cluster. Thus, when Φ^{o} = 0.314, a

50% reduction in C_1 results in a maximum reduction of 10% in the gas temperature and a maximum increase of 20% in the mass fraction of the evaporated compound in the outer third of the cluster, This effect is expected to become less important at Φ^o increases.

6.11 Effect of the small scale turbulence

As mentioned in 2., the small scale turbulence has been modeled here globally through a turbulent viscosity which is proportional to a constant C_T. By varying C_T one can explore the effect of the azimuthal drop motion which gives rise to these small scale turbulent features.

Thus, calculations were performed for $\Phi^o = 0.314$ with $C_T = 10^{-2}$ and $C_1 = 7 \times 10^{-2}$ in order to account for a factor of five turbulence reduction both in the interior of the cluster and at its boundaries. The most obvious results of this turbulence reduction are the substantial decrease *(1470)* in the gas temperature towards the outer part of the cluster and at the outer edge, the formation of a peak in the class drop number densities at the inner cluster boundary, the reduction in the drop number density at the outer cluster boundary, a more uniform profile of the total drop number density, including a reduction in the gradients at the outer cluster boundary, and an increased drop centrifugation.

The gas temperature reduction is a consequence of the decreased heat transfer from the ambient to the cluster through the reduction of C_1. This in turn affects the drop temperature and further the residual drop radius at the outer cluster edge. The larger drop size at the outer cluster edge together with a larger drop radial velocity resulted in increased drop centrifugation. This interpretation is corroborated by the larger value of the angle made by the velocity vector with the tangent at a fixed radial location.

The formation of a peak in the class number densities is associated with the tendency of the consecutive coordinate rings that bound the drops between radial locations to become thinner as C_T is smaller. Examination of plots of radial locations versus time reveals that whereas in the baseline calculation the distance between consecutive radial locations increases with time or remains constant, now this still holds everywhere but at the inner cluster edge where the distance between consecutive rings becomes smaller with time. This points out that small scale turbulence plays the important role of dispersing the drops at the microscale.

6.12 Effect of the initial drop number density distribution.

In order to understand the effect of the initial drop number distribution, parameters q_j and α_j (see Eqs. 51 and 53c) have been varied so as to change the width and the location of the peak of the distribution. Thus, in one calculation $q_1 = 2.5$ and $\alpha_1 = 0.25$ whereas q_2 and α_2 retain their baseline values of 0.5 and 0.5 respectively, whereas in another calculation $q_1 = q_2 = 2.5$ and $\alpha_1 = \alpha_2 = 0.5$. Additionally, a calculation with a monodisperse collection of drops has also been performed with $q = 10^3$ and $R^o_d = 2 \times 10^{-3}$ cm so as to simulate a unifcwmly-distributed, nondisperse cluster such as studied previously by Bell an and Harstad (1990). In all these calculations $\Phi^o = 0.314$ and the other initial conditions are those of the typical calculation (see Fig. 3 caption).

Results from a monodisperse, uniformly-distributed collection of drops are illustrated in Fig. 30. They show nonuniformities quickly developing in the gas temperature and drop size, thereby invalidating the monodisperse assumption in time dependent calculations for initially dense sprays. The drop number density (Fig. 30a) appears to remain uniform n the central

part of the cluster, although nonuniformities develop towards the inner and outer boundaries of the cluster. Thus, if boundary effects are of no concern, the uniformity assumption for the drop number density might have some validity for engineering calculations. These results are consistent with those found for a binary size distribution in 6.2.

The effect of larger gradients in the initial drop number distribution was investigated by performing calculation with $q_1 = q_2 = 2.5$ (the baseline value is 0.5). For this new drop number distribution whose evolution is shown in Fig. 31, there exist extremely dense regions of drops in the center of the cluster, where the drops are just a few diameters apart. Examination of the drop size distribution shows that in the central part of the cluster the residual drop sizes are larger, and thus that it takes longer for the drops the evaporate.

An interesting observation is that even for these more nonuniform initial drops size distributions, time relaxation also produces a distribution that in the majority of the cluster (excluding about 15-20% where edge effects are important) is an increasing function of the radial location, although the gradients are now larger.

Another aspect of the initial drop number distribution has been explored by having different initial maxima and different skewness for the two initial size classes. The values of $\alpha_1 = 0.25$, $\alpha_2 = 0.5$, $q_1 = 2.5$ and $q_2 = 0.5$ were chosen, thereby rendering the initial drop number distribution for initial-size-class-1 narrower and with a maximum closer to the inner cluster boundary. Plots of the evolution of the drop number distribution are illustrated in Fig. 32, whereas plots of ratio of the average drop distance between the centers of two adjacent drops, the gas temperature and the mass fraction of the evaporated compound are depicted in Fig. 33. The minimum in the gas temperature corresponds to a maximum in the

drop number density of initial-size-class-2. The different locations of the maxima for the initial size class drop number densities produce a monotonic total drop number density with a maximum located at the same radial position as that for the more numerous initial-size-class-1 drops. In fact, it appears that initial-size-class-2 drops are mostly located near the inner and outer peripheries of the cluster, while most initial-size-class-1 drops are located in the central part of the cluster. The low gas temperature in the central part of the cluster affects drop evaporation as shown in Fig. 34; pockets of relatively large size drops survive for an extended time in both initial size classes, and when the calculation is terminated there is still an unevaporated pocket of initial-size-class-2 drops in the minimum temperature region.

These selected results of calculations with different initial drop number density profiles illustrate only a few of the possible configurations. However, what emerges from this limited study of the initial drop number density profiles, is that for the purpose of comparing numerical results and experimental observations, and accurate prediction of the characteristics of the cluster of drops is highly dependent upon the accuracy of the initial conditions.

7. SUMMARY AND CONCLUSIONS

A model has been developed to describe the dynamics and evaporation of a polydisperse cluster of liquid drops in a gaseous, cylindrical, axisymmetric, infinite vortex. Important features of the model are the two-way coupling between gas and drops, both dynamically and thermodynamically, and the ability of the model to account for multiparticle interactions in terms of their motion, heating and evaporation. Thus, both dense and dilute clusters of

drops can be described by this model. The concept of denseness is based upon the nondimensional ratio of the average distance between the centers of adjacent drops divided by the average diameter of the drops. Previous studies have shown that the dense regime starts at volumetric liquid/gas ratios as small as 3×10^{-4} while the very dense regime starts at liquid/gas volumetric ratios of 10^{-3}. For these volumetric ratios, numerical results have shown departures from the dilute results in the case of monodisperse, uniformly distributed clusters of drops (Bellan and Harstad, 1987, 1990; Harstad and Bellan, 1991).

In contrast to the standard technique of partitioning the drop size distribution into size bins and following the same bins in time, here it is only the initial drop size distribution that is partitioned into bins and each initial size class thus defined develops its own, continuous, drop size distribution which is discretized in a system of coordinates moving with the initial size class.

Results from calculations made by varying an extended number of parameters showed that:

(1) For dilute clusters of drops, the drop number distribution relaxes towards a uniform distribution in most of the cluster, excluding the inner and outer periphery.

(2) For dense clusters of drops, an initially nonuniform drop number distribution remains nonuniform throughout the lifetime of the evaporating drops, but an initially uniform drop number distribution remains uniform in most of the clusters excluding its peripheries.

(3) The drop size distribution cannot be assumed uniform for moderately dense, dense or very dense clusters of drops, even for a monodisperse initial drops size distribution,

(4) Drop dynamics and evaporation is controlled by the air/liquid mass ratio in the inner half of the cluster and by the drop size distribution in the outer half of the cluster.

(5) The behavior of the outer region of the cluster is controlled by the solid body rotation of the gas, whereas the behavior of the inner region of the cluster is controlled by the irrotational motion of the gas.

(6) The initial drop solid body rotation controls the drop number density distribution, the drop size distribution and the gas temperature within the cluster.

(7) Polydispersity increases the maximum of the mass fraction of the evaporated compound within the cluster and enhances penetration of the evaporated compound into the ambient, For the purpose of spray combustion it is recommended to have a proportionally larger amount of small drops into the spray to enhance evaporation; the larger drops will be responsible for centrifugation and thus penetration of the vapor into the ambient.

(8) Dense clusters of drops have more control parameters influencing their behavior than dilute clusters of drops.

(9) Transport from the ambient to the cluster, and small scale turbulence within the cluster have important effects upon the drop number distribution, drop size distribution and gas temperature within the cluster.

(lo) Knowledge of an accurate drop number distribution for each initial size class is essential for being able to make quantitatively accurate predictions of the important features of drop behavior.

The study presented here has not addressed, starting from first principles, the question of the development of small scale turbulence due to the drops motion. This important

problem, as well as a more detailed description of the outer boundary region of the cluster and the adjacent ambient region, remain to be considered in further work.

This research has been conducted at the Jet Propulsion Laboratory under sponsorship from the U.S. Air Force Wright Laboratory, Aero Propulsion and Power Directorate, with Dr. T. Jackson serving as contract monitor, under an agreement with the National Aeronautics and Space Administration.

APPENDIX I: SINGULARITY ANALYSIS OF SOLUTIONS OF THE DROPS CONSERVATION EQUATIONS

For simplicity, the case of a single drop size class without turbulent diffusion or $\hat{p}$ is examined here. The goal is to determine whether the system of equations possesses a nonsingular (regular) solution for any initial conditions, and if not to identify a set of initial conditions for which the solution is regular, at least for short times.

Following the equations given in 3A, the drops equations are

$$\frac{dr}{dt} = u_{dr} \tag{A1}$$

$$\frac{du_{dr}}{dt} = \frac{u_{d\theta}^2}{r} - \nu_s (u_{dr} - u_{gr}) \tag{A2}$$

$$\frac{d\Gamma_d}{dt} = -\nu_s (\Gamma_d - \Gamma_g) \tag{A3}$$

where

$$\Gamma_d \equiv r u_{d\theta} \quad , \quad \Gamma_g \equiv r u_{g\theta} \tag{A4}$$

and

$$\frac{\partial n}{\partial t} + \frac{1}{r} \frac{\partial}{\partial r} (r u_{dr} n) = 0 \tag{A5}$$

The Lagrangian radial coordinates associated with the drop are r = r (t, r^o) where r" is the

position at t = O, and the initial condition for the radial velocity is $u_{dr}(0, r")$.

If a solution of this system of equations exists at $t > 0$, then that means that there exists a one-to-one transformation between r and r" and the mapping $r^o \rightarrow r$ is nonsingular. The Jacobian of this mapping is

$$J \equiv \frac{\partial r}{\partial r^0} = J(t, z\text{-}") \qquad \textbf{(A6)}$$

with J (O, r") = 1.

For specified $u_{g0}(t, r) = u_{g0}(t, r")$, Eq. (A3) can be solved to yield

$$\Gamma_d = \Gamma_d^o \exp\left(-\int_o^t \nu_s dt'\right) + \int_o^t \nu_s \Gamma_g \exp\left(-\int_{t'}^t \nu_s \, dt''\right) dt' \qquad \textbf{(A7)}$$

Since for low Reynolds numbers $\nu_s = D_s/R_d^2$, where $D_s = 9\mu_g/(2\rho_l) \sim 10^{-4}$ cm^2/sec and $R_d = O(10^{-3})$cm, then $\nu_s >> 1$. Eq.(A7) shows that

$$if \int_o^t \nu_s \, dt' << 1 \quad , \quad then \; \Gamma_d \sim \Gamma_d^o = r^o u_{d0}^o(r^o)$$

$$if \int_o^t \nu_s \, dt' >> 1 \quad , \quad then \quad \Gamma_d \sim \Gamma_g \quad , \quad u_{d0} \sim u_{g0}$$

The momentum equations can be expressed in term of J by noticing that for a thin drop ring, Δr^o, initially located at r", at t > O

$$\Delta r = J\,\Delta r^{o} \tag{A8a}$$

$$\Delta\frac{dr}{dt} = \Delta u_{dr} = \frac{dJ}{dt}\,\Delta r^{o} \tag{A8b}$$

$$\Delta\frac{du_{dr}}{dt} = \frac{d^{2}J}{dt^{2}}\Delta r^{o} \tag{A8c}$$

$$\Delta u_{d\theta} = \frac{\partial u_{d\theta}}{\partial r}\,J\,\Delta r^{o} \tag{A8d}$$

$$\Delta u_{gr} = \frac{\partial u_{gr}}{\partial r}\,J\,\Delta r^{o} \tag{A8e}$$

where Δ represents the difference between the values of the variables at the two extreme positions defining a ring. This means that from Eq. (A2)

$$\Delta\frac{du_{dr}}{dt} = \frac{2\,u_{d\theta}}{r}\,\Delta u_{d\theta} - \left(\frac{u_{\infty}}{r}\right)^{2}\Delta r - \nu_{s}(\Delta u_{dr} - \Delta u_{gr}) \tag{A9}$$

The above equation can be interpreted as a differential equation for J

$$\frac{d^{2}J}{dt^{2}} + \nu_{s}\frac{dJ}{dt} + \left(\omega^{2} - 2\omega\frac{\partial u_{d\theta}}{\partial r} - \frac{\partial u_{a}}{\partial r}\right)J = 0 \tag{A10}$$

where

$$\omega = \frac{d\theta}{dt} = \frac{u_{d\theta}}{r} \qquad (A11)$$

θ is the azimuthal angle change and for short times $\omega = r^{o}u^{o}_{d\theta}/r^{2}$.

Equation (A5) gives

$$\frac{d}{dt}\int_{\Delta r} nr\,dr = 0 \qquad (A12)$$

$$nr\Delta r = n^{o}\, r^{o}\Delta r^{o} \qquad (A13)$$

or

$$nrJ = n^{o}\, r^{o} \qquad (A14)$$

Also,

$$r = \int_{0}^{r^{o}} J(t, r^{o})\, dr^{o}. \qquad (A15)$$

The gas energy equation implies that u_{gr} depends upon n and according to the above relationships relating n to J, u_{gr} depends upon J. Note thus that the coefficient of J in Eq.(A10) depends upon J, and thus that it is very difficult to obtain a solution for J. However, one may observe that J will have an oscillatory form with a damping component. Depending upon the relative magnitude of the damping component with respect to the frequency of the oscillation, J might or not become null during the lifetime of the drops.

A sufficient condition for J to be non null is that Eq. (A1O) be quasi-steady; thus J is a strictly positive constant and

$$\omega^2 - 2\omega \frac{\partial u_{g\theta}}{\partial r} - v_s \frac{\partial u_{gr}}{\partial r} = 0 \qquad \text{(A16)}$$

Note that if $u^o_{dr} = O$, then $(dJ/dt)^o = O$. $(d^2J/dt^2)^o = O$ if $(du_{dr}/dt)^o = A^o$, where A^o is a constant. Using the momentum equation one obtains

$$\frac{(u^o_{g\theta})^2}{r^o} = A^o - v^o_s \, u^o_{gr} \qquad \text{(A17)}$$

In order to satisfy the above relationship for all r, $A^o \geq v^o$, max (u^o_{gr}) is chosen.

REFERENCES

Abramzon, B. and Sirignano, W. A. 1989 Droplet vaporization model for spray combustion. Int. J. Heat Mass Transfer, 32, 1605-1618.

Bellan, J. and Cuffel, R. 1983 A theory of non dilute spray evaporation based upon multiple drop interactions. Combust. and Flame, 51, 55-67.

Bellan, J. and Harstad, K. 1987 The details of the convective evaporation of dense and dilute clusters of drops. Int. J. Heat Mass Transfer, 30, 6, 1003-1093.

Bellan, J. and Harstad, K. 1988 Turbulence effects during the evaporation of drops in clusters. Int. J. Heat Mass Transfer, 31, 8, 1655-1668.

Bellan, J. and Harstad, K. 1990 The dynamics of dense and dilute clusters of drops evaporating in large, coherent vortices. 23rd Symp. (Int.) on Combustion, 1375-1381, Orleans.

Chang, C. and Powell, R. L. 1993 Dynamic simulation of bimodal suspensions of hydrodynamically interacting spherical particle. J. Fluid Mech., 253, 1-25.

Chung, J.N. and Troutt, T.R. 1988 Simulation of particle dispersion in an axisymmetric jet. J. Fluid Mech., 186, 199-222.

Cliffe, K. A. and Lever, D. A. 1985 Isothermal flow past a blowing sphere. Int. J. Numer. Meth. Fluids, 5, 709-725.

Crowe, C. T., Chung, J. N. and Troutt, J.R. 1988 Particle mixing in free shear flows. Prog. Energy Combust. Sci., 14, 171-194.

Crowe, C. T., Chung, J. N., and Troutt, J. R. 1993 Particle dispersion by organized turbulent structures, Particulate Two Phase Flows. ButterWorth, Ed. M. Roco, Chapt. 18.

Durlofsky, L., Brady, J. F. and Bossis, G. 1987 Dynamic simulation of hydrodynamically interacting particles. J. Fluid Mech., 180, 21-49.

Elghobashi, S. and Truesdell, G. C. 1992 Direct simulation of particle dispersion in a decaying isotropic turbulence. J. Fluid Mech. 242,655-700.

Elghobashi, S. and Truesdell, G. C. 1993 On the two-way interaction between homogeneous turbulence and dispersed solid particles; Part I: turbulence modification. Phys. Fluids *4* 5(7), 1790-1801

Hardalupas, Y., Taylor, A. M. K, P. and Whitelaw, J. H. 1990 Velocity and size characteristics of liquid-fueled flames stabilized by a swirl burner. Proc. R. Sot. Lond., A428, 129-155.

Hardalupas, Y., Taylor, A. M. K. P. and Whitelaw, J. H. 1992, Particle dispersion in a vertical round sudden-expansion flow, Phil. Trans. R. Soc. Lond., A341, 411-442.

Harstad, K. and Bellan, J. 1991 A model of the evaporation of binary-fuel clusters of drops. Atomization and Sprays, 1, 367-388.

Hidy, G.M. and Brock, J. R. 1970, The dynamics of aerocoloidal systems, International Reviews in Aerosol Physics and Chemistry, Vol 1, Pergamon Press.

Lazaro, B. J. and Lasheras, J.C. 1989 Particle dispersion in a turbulent, plane, free shear layer. Phys. Fluids A, 1(6), 1035-1044.

Lazaro, B.J. and Lasheras, J.C. 1992 Particle dispersion in the developing free shear layer. Part 1. Unforced flow. J. Fluid Mech., 235, 143-178.

Lazaro, B. J. and Lasheras, J. C. 1992 Particle dispersion in the developing free shear layer. Part 2, Forced flow. J. Fluid Mech., 235, 197-221.

Longmire, E. K. and Eaton, J. K, 1992 Structure of a particle-laden round jet. J. Fluid Mech. ,236, 217-257.

McDonnel, V. G., Adachi, M. and Samuelsen, G.S. 1992 Structure of reacting and non-react ing swirling air-assisted sprays. Comb. Sci. and Tech., 82, 225-248.

Mizutani, Y., Nakabe, K.., Fuchihata, M., Akamatsu, F., Zaizen, M., and El-Emam, S.H. 1993 Spark-ignited spherical flames propagating in a suspended droplet cloud. Atomization and Sprays, 3, 125-135.

Parthasarathy, R.N. ancl Faeth, G.M. 1990 Turbulence modulation in homogeneous dilute particle-laden flows. J Fluid Mech., 220, 485-514.

Parthasarathy, R.N. and Faeth, G.M. 1990 Turbulence dispersion of particles in self-generated homogeneous turbulence J Fluid Mech 220,515-537.

Raju, M.S. and Sirignano, W.A. 1990 Interaction between two vaporizing droplets in an intermediate Reynolds number flow. Phys. Fluids A., Z?(10), 1780-1796.

Rudoff, R. C., Brena de le Rosa, A., Sankar, S, V., and Bachalo, W. D. 1989 Time analysis of polydisperse sprays in complex turbulent environments. 27th Aerospace Sciences Meetnig, paper AIAA-89-0052.

Schreck, S. and Kleis, S. J. 1993 Modification of grid-generated turbulence by solid particles. J. Fluid Mech., 249, 665-688.

Squires, K. D. and Eaton, J. K. 1990 Particle response and turbulence modification in isotropic turbulence. Phys. Fluids A, 2(7), 1191-1203.

Squires, K. D. and Eaton, J. K., 1991, Preferential concentration of particles by turbulence. Phys. Fluids A, 3(5), 1169-1178.

Tal, R., Lee, D. N. and Sirignano, W.A. 1983 Hydrodynamics and heat transfer in sphere assemblages: multisphere cylindrical cell models. Int. J. Heat Mass Transfer, 26(9), 1265-1273.

Zhang, X., Davis, R.H. and Ruth, M.F. 1993 Experimental study of two interacting drops in an immiscible fluid. J. Fluid Mech., 249, 227-239.

Table 1

THERMOPHYSICAL PROPERTIES USED IN THE CALCULATIONS

n-decane

heat capacity of liquid C_{pl} = 0.523 cal/g°K
liquid density ρ_l = 0.734 g/cm^3
liquid conductivity k_l = 2.5 x 10^{-4} cal/cm°K sec
liquid viscosity μ_l = 2.6 x 10^{-2} g/cm sec
liquid diffusivity D_{ml} = 4 x 10^{5} cm^2/sec
latent heat of evaporation L_{evap} = 73.92 cal/g
heat capacity of vapor C_{pvap} = 0.4 cal/g°K
normal boiling point temperature T_b = 447.7°K
molecular weight W = 142 g/mole

air

C_{pa} = 0.241 cal/g°K
W_{ag} = 28.9 g/mole
$\mu^{\circ}_{g\infty}$ = 4.2x 10^{4} g/cm sec at lOOOK
Pr_g = 0.8

$AC_p = C_{pl} - C_{pg}$ = 0.0292 Cal/g°K, fitted for the saturation pressure curve

Table 11

Line Symbol	Time, sec
———.—.....>...-.". . ..>. -..	6.99 $\times 10^{-5}$ sec
———————————	7.69 $\times 10^{-4}$ sec
—-.-—————— . . . . . ——	1.47 x 10^{-3} sec
``	2.17 $\times 10^{-3}$ sec
——— ——— — — ——— ———	2.87 $\times 10^{-3}$ sec
———————————	3.56 $\times 10^{-3}$ sec
— — — . - ——— — -	4.26 $\times 10^{-3}$ sec
— — . — — —	5.66 $\times 10^{-3}$ sec
——.——. — -——.——.——	7.06 x 10^{-3} sec
------- ------- ——.—.	8.39 $\times 10^{-3}$ sec

FIGURES

Figure 1. Sketch of a binary size configuration and of the coordinate systems.

Figure 2. Illustration of an individual drop coordinate system.

Figure 3. Ratio of the average drop diameter by the average distance between the centers of two adjacent drops versus the coordinate associated with the gas in the cluster at different times. Initial parameters are: $\Phi^o = 0.314$, $T^o_{g_0} = 1000K$, $T^o_{g_0} = 350K$, $R^o_1 = 2 \times 10^{-3}$ cm, $R^0_2 = 2{,}5 \times 10^{-3}$ cm, max $(n^*_1) = 104$cm-3, max $(n^o_2) = 3 \times 10^3 cm^{-3}$, $\alpha_1 = \alpha_2 = 0.5$, $q_1 = q_2 = 0.5$, $R^{\prime\prime}_c = 2$ cm, $b_{i1} = b_{i2} = 0.1$, initial drop acceleration for both classes is 20 cm/sec^2, null initial drop spin rate for both initial size classes, $u^o_{g0} = 100/r_c cm/sec^2$, $C_T = 5 \times 10^{-2}$, $C_1 = 0.35$. Refer to Table II for the legend.

Figure 4. Ratio of the average distance between the centers of two adjacent drops to drop radius of initial-class-size-l (4a) versus the coordinate associated with initial-class-size-l at different times. The equivalent plot for initial-size-class-2 is in (4b). Initial parameters are those listed in the Figure 3 caption. Refer to Table 11 for the legend.

Figure 5. Total drop number density (5a), drop number density of initial-size-class-1, (5b) and drop number density of initial-size-class-2 (5c) versus the gas coordinate in the cluster at various times. Initial parameters are those listed in the Figure 3 caption. Refer to Table H for the legend.

Figure 6. Residual drop radius for initial-size-class-1 (6a) and initial-size-class-2 (6b) versus the gas coordinates in the cluster at various times. Initial parameters are those listed in the Figure 3 caption. Refer to Table 11 for the legend.

Figure 7. Gas temperature in the cluster versus the gas coordinate in the cluster at different times. Initial parameters "are those listed in the Figure 3 caption. Refer to Table II for the legend.

Figure 8. Mass fraction of the vaporized liquid (n-decane) in the gas phase versus the gas coordinate in the cluster at different times. Initial parameters are those listed in the Figure 3 caption. Refer to Table 11 for the legend.

Figure 9. Variation of the ratio of the average drop radius by the average radius of the sphere of influence versus the radial coordinate for air/liquid mass ratios of 0.314, 0.785 and 1.57 (9a, 9b, 9c). Refer to Table II for the legend.

Figure 10. Total drop number density versus the radial coordinate for $\Phi^o = 0.314$, 0.785 and 1.57 (lOa, 10b, 10c). Refer to Table 11 for the legend.

Figure 11. Comparison of the variation of the radial drop velocity *versus the* radial coordinate (Fig. 1 la) and the tangential drop velocity versus the radial coordinate (Fig 11b) for Φ^o = 0.314(i), 0.785(ii) and 1.57(iii). The values shown are for initial- size- class- 1 for which R"= 2.0 x 10^{-3} cm. Refer to Table II for the legend.

Figure 12. Development of the gas temperature profile for Φ^o = 0.314, 0.785 and 1.57.

Figure 13. Residual drop radius for initial-size-class-1 (Fig. 13a) and initial-size-class-2 (Fig. 13b) for Φ^o = 0.314(i), 0.785(ii) and 1.57(iii). Refer to Table II for the legend.

Figure 14. Distribution of mass fraction of the evaporated compound for Φ^o = 0.314,0.785 and 1.57 (14a, 14b, 14c). Refer to Table 11 for the legend.

Figure 15. Drop' number density distribution for an initially monodisperse cluster of drops with Φ^o = 0.314, R"= 2.0 x 10^{3} cm. Refer to Table 11 for the legend.

Figure 16. Drop number density variation for bimodal distributions having R^o_1= 2 x 10^{3} cm and R^o_2= 3 x 10^{3} cm for Φ^o = 0.314 (16a) and Φ^o = 0.785 (16b). Refer to Table 11 for the legend.

Figure 17. Residual radius for initial-size-class-1 (17a) and initial-size-class-2 (17b) versus the radial coordinate when Φ^o = 0.314, R^o_1= 2 x 10^{-3} cm and R^o_2= 3 x 10^{-3} cm. Refer to Table II for the legend.

Figure 18. Comparison of gas temperature profiles at selected times for two bimodal size distributions when Φ^o = 0.314.

Figure 19. Evolution of the mass fraction profile of the evaporated compound when Φ^o = 0.314, R^o_1= 2 x 10^{-3} cm and R^o_2= 3 x 10^{-3} cm. Refer to Table H for the legend.

Figure 20. Evolution of the total and partial drop number densities for an initially trimodal drop size distribution with R^o_1= 2 x 10^{-3} cm, R^0_2= 3 x 10^{-3} cm, $R"_3$= 2 x 10^{3} cm and Φ^o = 0.314 (total, 20a; initial-size-class-1, 20b; initial-size-class-2, 20c; initial-size-class-3, 20d). Refer to Table II for the legend.

Figure 21, Gas temperature evolution for the initially trimodal size distribution described in the caption of Fig, 20. Refer to Table II for the legend.

Figure 22. Evolution of the mass fraction of the evaporated compound for the initially trimodal size distribution described in the caption of Fig. 20. Refer to Table 11 for the legend.

Figure 23. Residual drop size distribution for the three initial size classes described in the caption of Fig. 20 (initial-size-class-1, 23a; initial-size-class-2, 23b; initial-size-class-3; 23c). Refer to Table II for the legend.

Figure 24. Mass fraction of the evaporated compound for a calculation where the air/liquid mass ratio is the same as in the baseline case, but $\max(n^{\circ}_1) = 3 \times 10^3\ cm^{-3}$ and $\max(n^{\circ}_2) = 10^4 cm^{-3}$. Refer to Table 11 for the legend.

Figure 25. Evolution of the gas temperature profile when $T^{\circ}_{g_0} = 300K$; all other initial parameters are those listed in the Fig. 3 caption. Refer to Table II for the legend,

Figure 26. Variation of the residual drop radius for the two initial size classes (class 1, 26a; class 2, 26b). The initial conditions are listed in Fig. 25 caption. Refer to Table II for the legend.

Figure 27. Distribution of the evaporated compound mass fraction for the initial conditions listed in the Fig. 25 caption. Refer to Table II for the legend.

Figure 28. Drop number density (28a and 28b) and residual radius (28c and 28d) profiles for $A^{\circ}_{g0} = 100\ cm^2/sec$ and $B^{\circ}_{g0} = 200$ see-l (28a and 28c), $A^{\circ}_{g0} = 100\ cm^2/sec$ and $B^{\circ}_{gT} = 200\ sec^{-1}$ (28b and 28d). All other parameters are listed in the Fig. 3 caption. Refer to Table II for the legend.

Figure 29. Drop number densities (total 29a; initial-size-class-1 29b; initial-size-class-229c) versus radial coordinate when $C_1 = 0.175$. All other parameters are listed in Fig. 3 caption. Refer to Table II for the legend.

Figure 30. Variation of the drop number density (30a), gas temperatures (30b), residual drop radius (30c) and average drop size divided by the average distance between drops (30d) for an initially monodisperse, uniform ($q_1 = 10^{-3}$) cluster. All other parameters are listed in Fig. 3 caption. Refer to Table II for the legend.

Figure 31. Drop number densities (total 31a; initial-size-class-1 31b; initial-size-class-231c) versus radial coordinate when $q_1 = q_2 = 2.5$. All other parameters are listed in Fig. 3 caption. Refer to Table II for the legend.

Figure 32. Drop number densities (total 32a; initial-size-class-1 32b; initial-size-class-232c) versus radial coordinate where $\alpha_1 = 0.25$, $\alpha_2 = 0.5$, $q_1 = 2.5$ and $q_2 = 0.5$. All other parameters are listed in Fig. 3 caption. Refer to Table II for the legend.

Figure 33. Average drop radius divided by average drop distance (33a), gas temperature (33b), and mass fraction of the evaporated compound (33c) for the parameters listed in Fig. 32 caption. Refer to Table II for the legend.

Figure 34. Residual radius of initial-size-class-1 drops (34a) and initial-size-class-2 (34b) for the parameters listed in Fig. 32 caption. Refer to Table H for the legend.

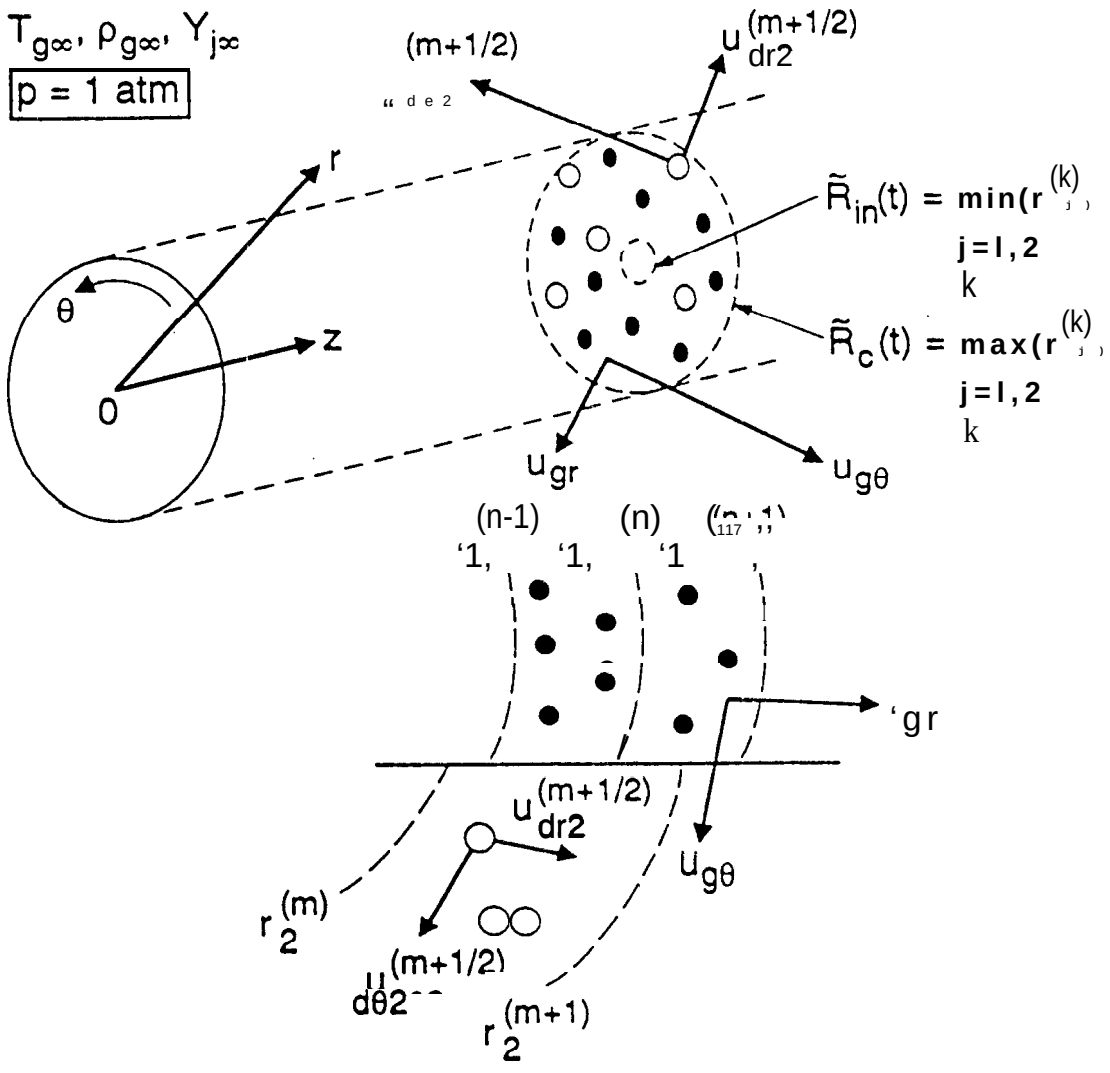
$T_{g\infty}$, $\rho_{g\infty}$, $Y_{j\infty}$
p = 1 atm
r
θ
z
0
u_{gr}
$u_{g\theta}$
$\tilde{R}_{in}(t) = \min_{j=1,2}(r_j^{(k)})$
$\tilde{R}_c(t) = \max_{j=1,2}(r_j^{(k)})$
(m+1/2)
(n-1)
(n)
(m)
(m+1)

Figure 1

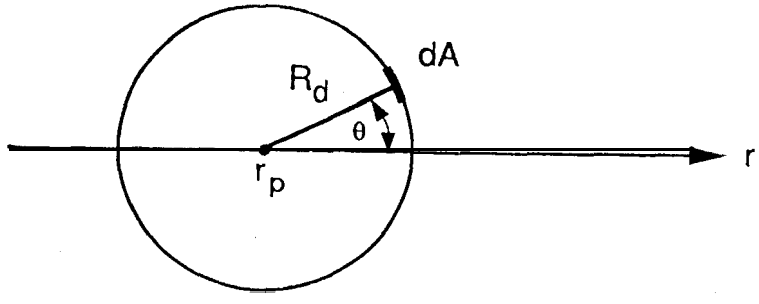

Figure 2

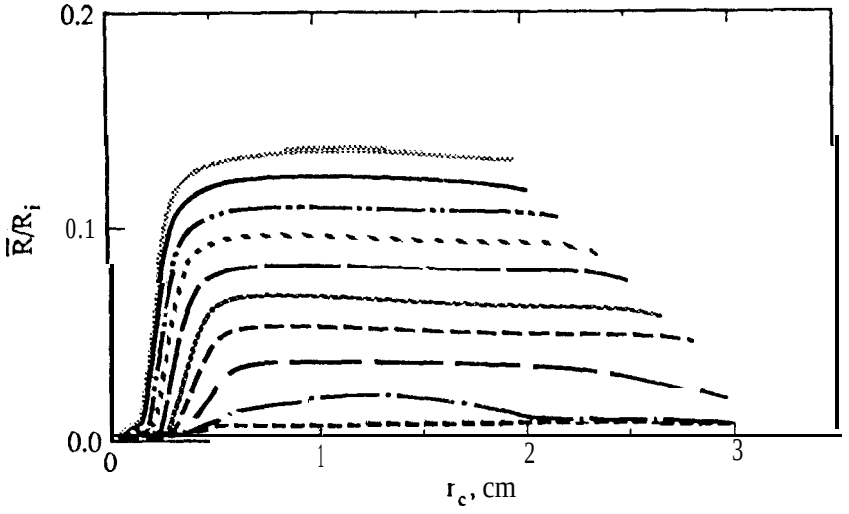

Figure 3

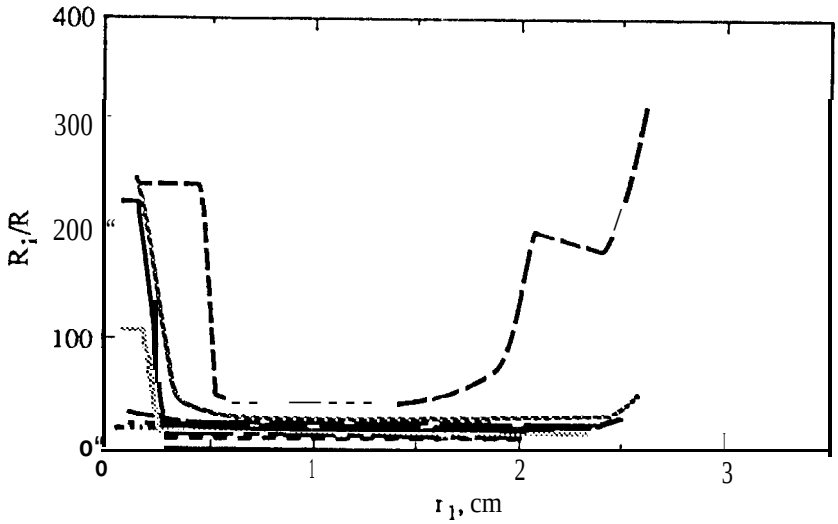

Figure 4a

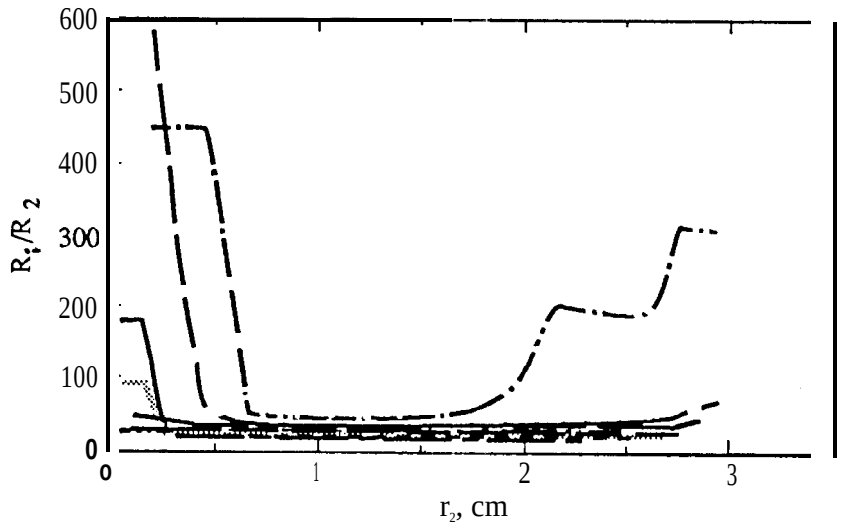

Figure 4b

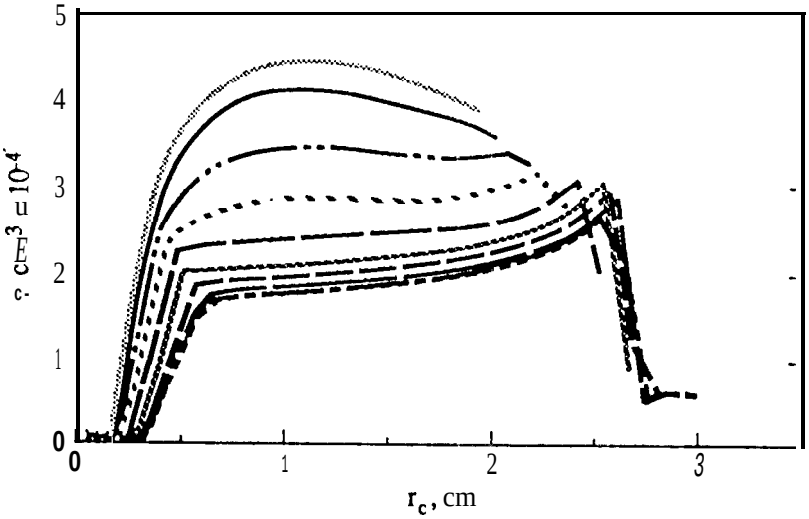

Figure 5a

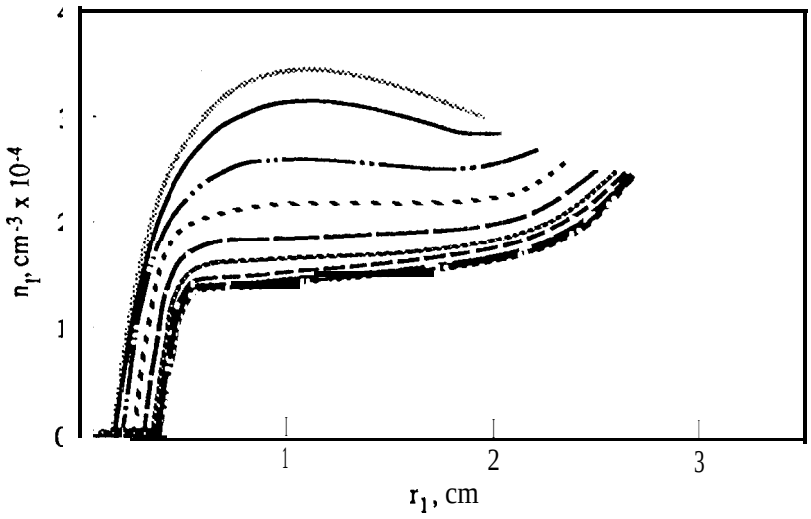

Figure 5b

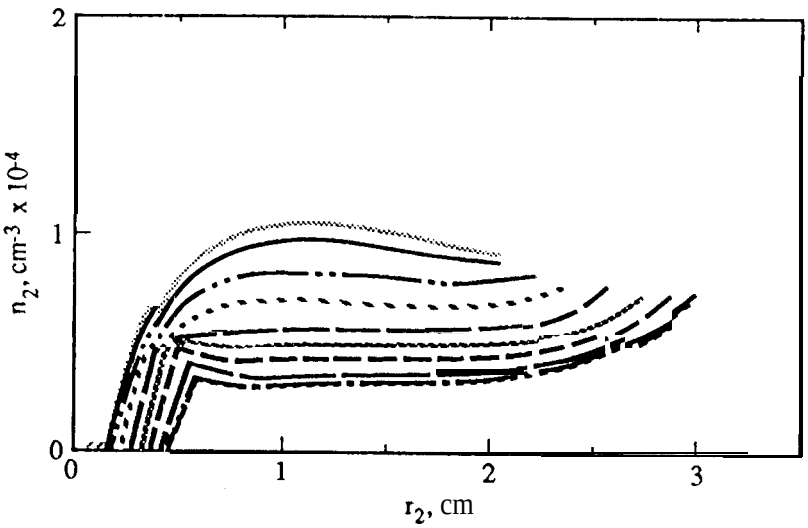

Figure 5c

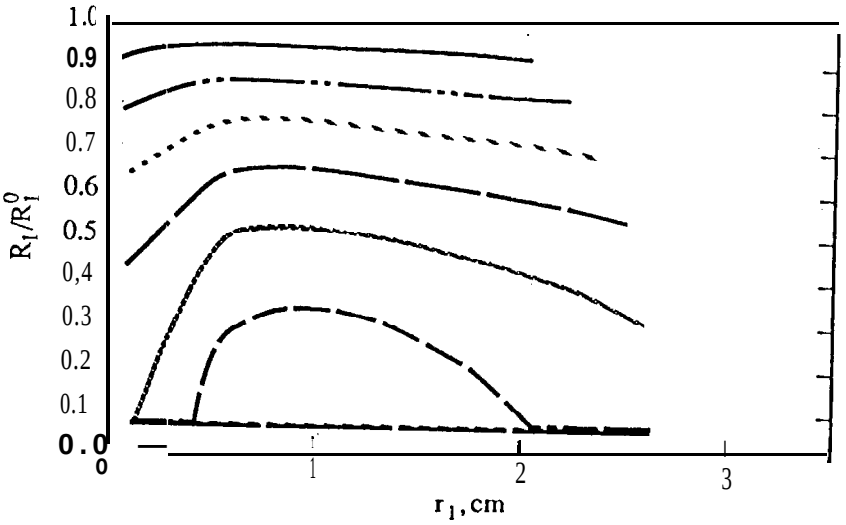

Figure 6a

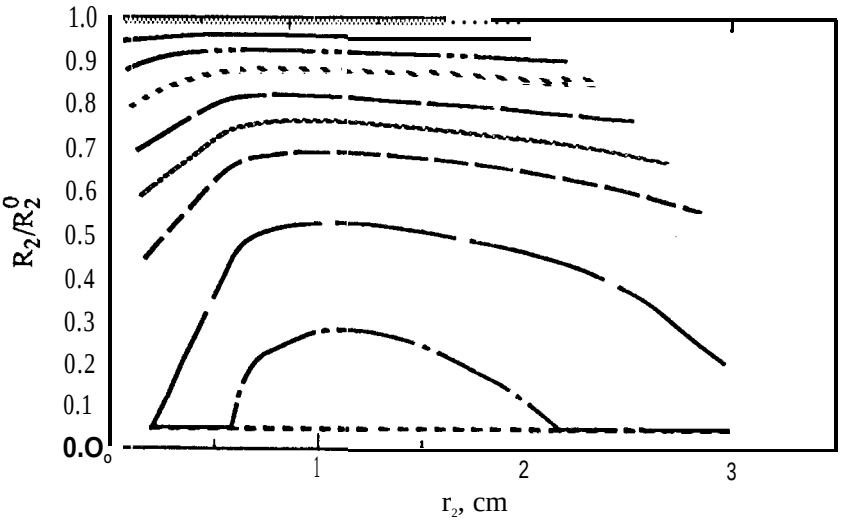

Figure 6b

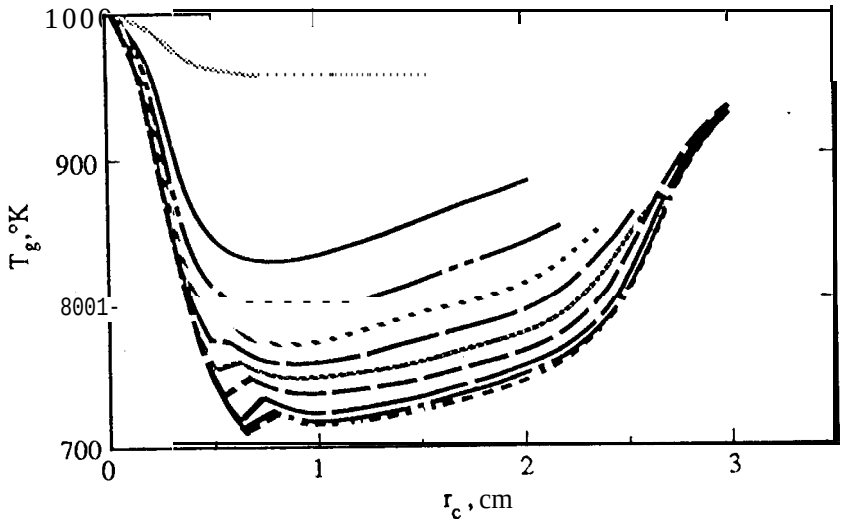

Figure 7

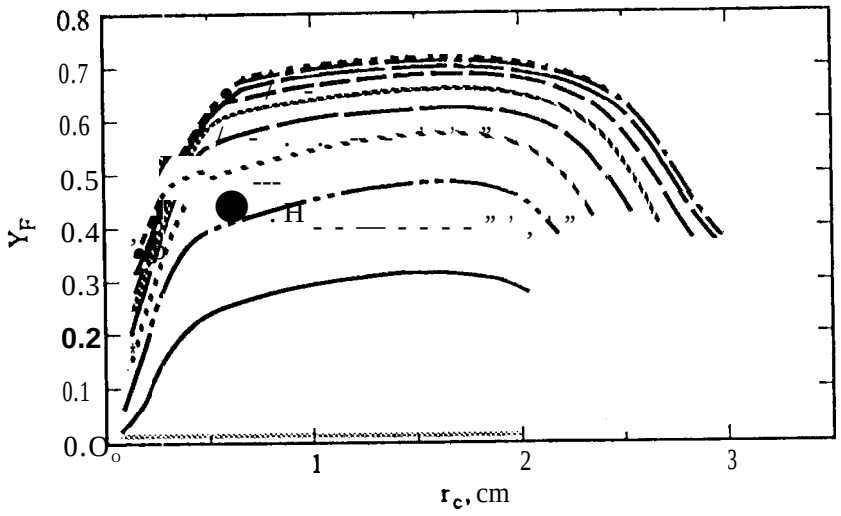

Figure 8

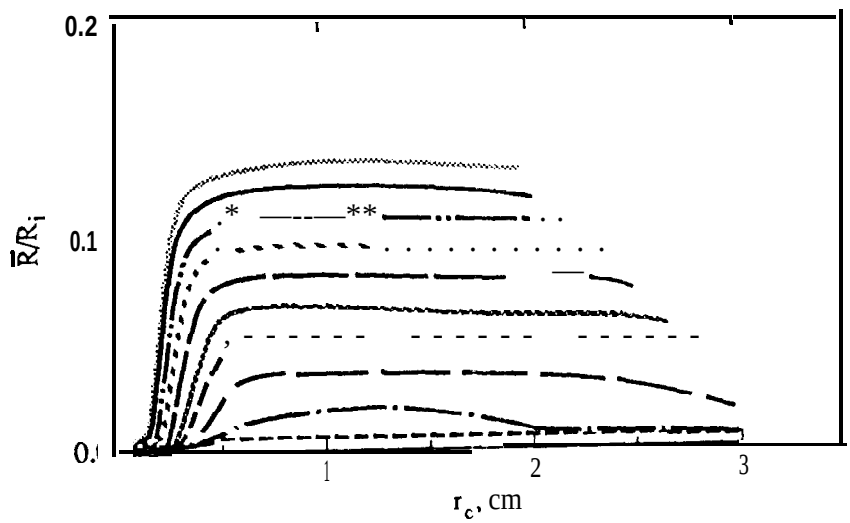

Figure 9a

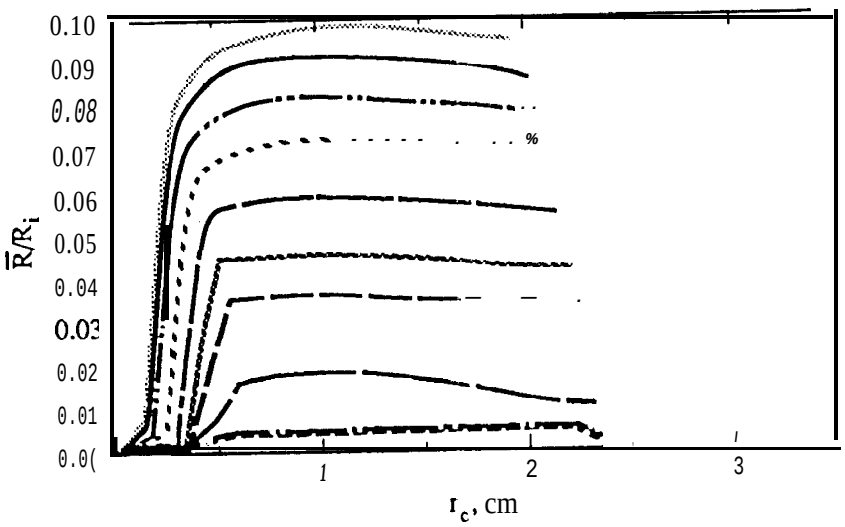

Figure 9b

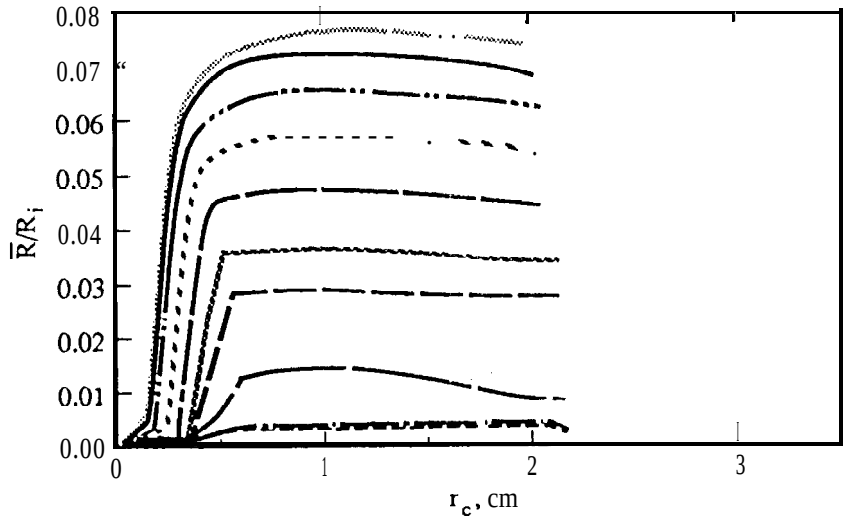

Figure 9c

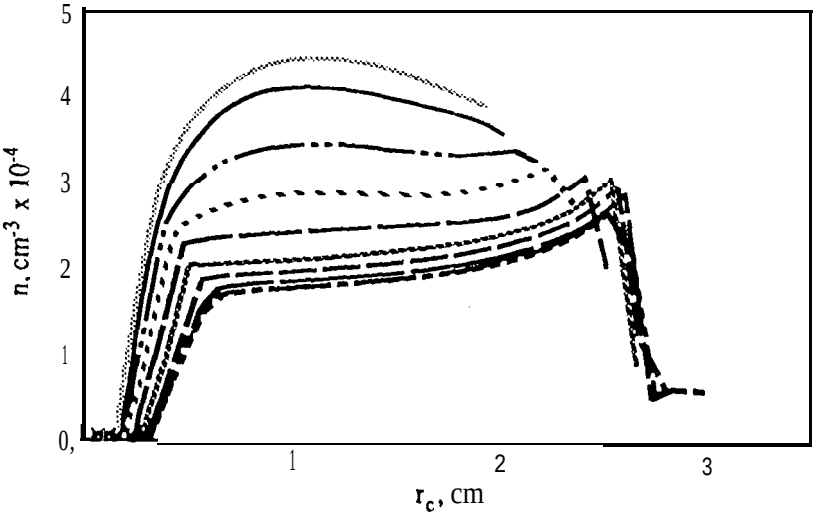

Figure 10a

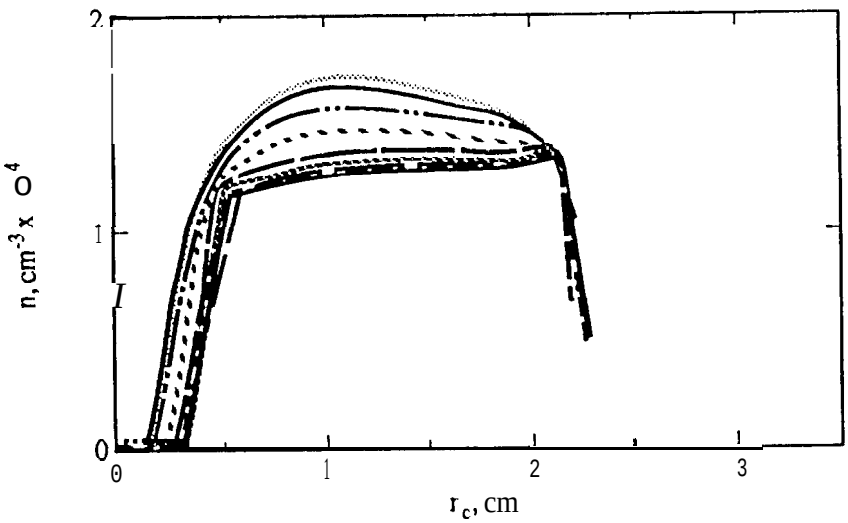

Figure 10b

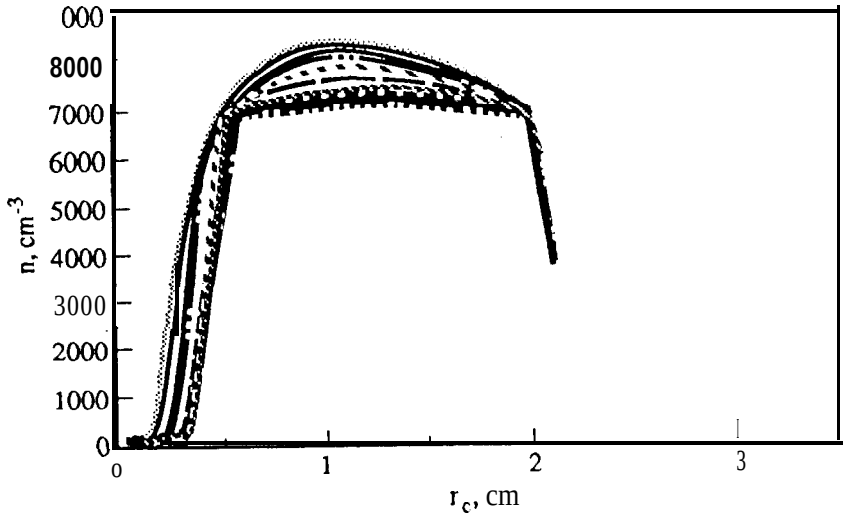

Figure 10c

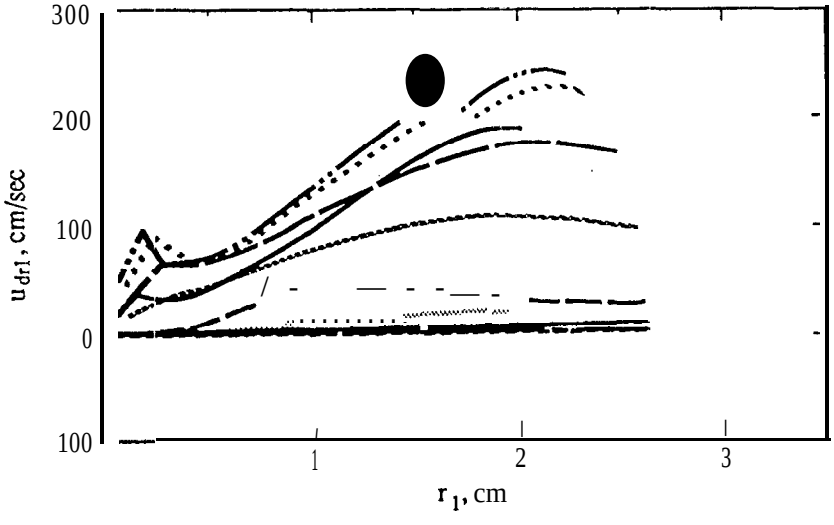

Figure 1 la (i)

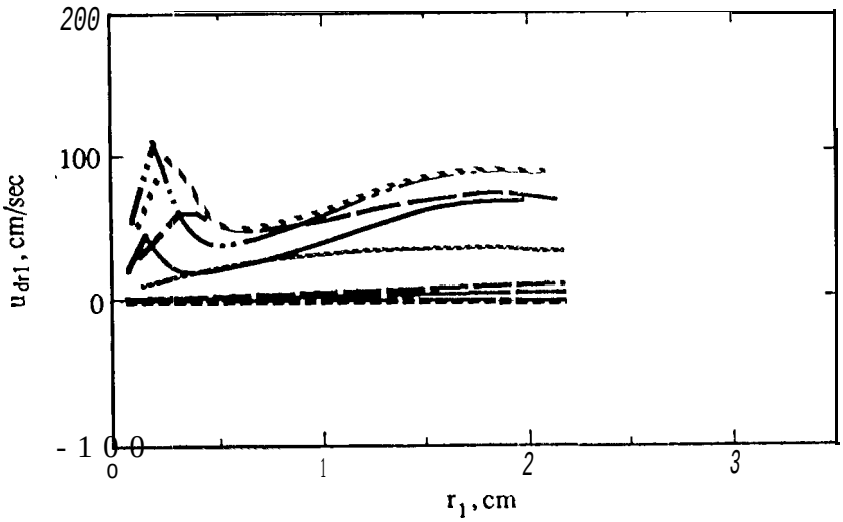

Figure 1 la (ii)

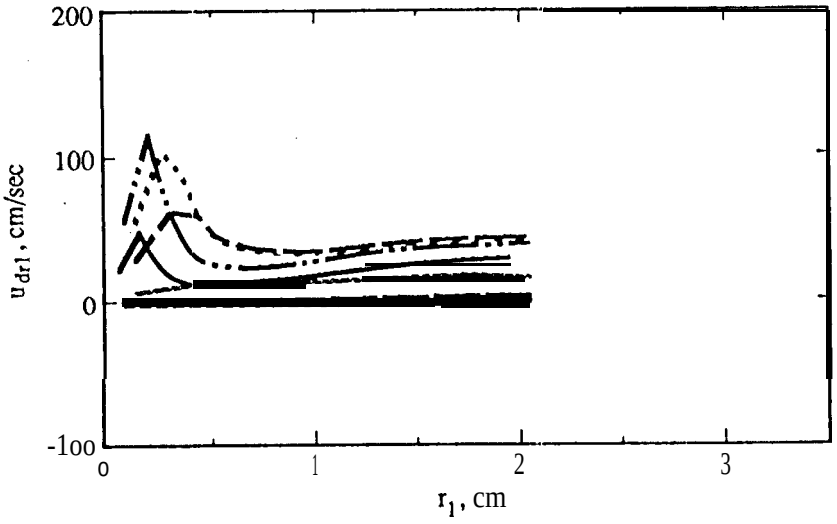

Figure 1 la (iii)

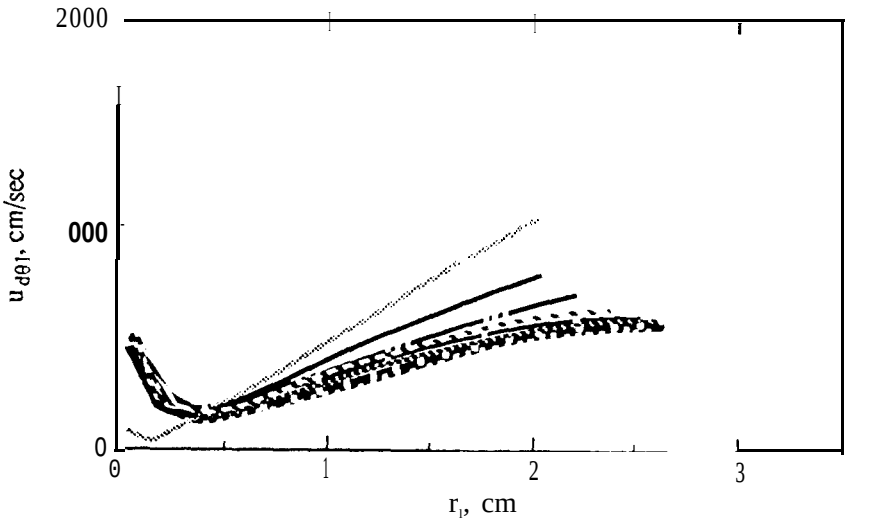

Figure 1 lb (i)

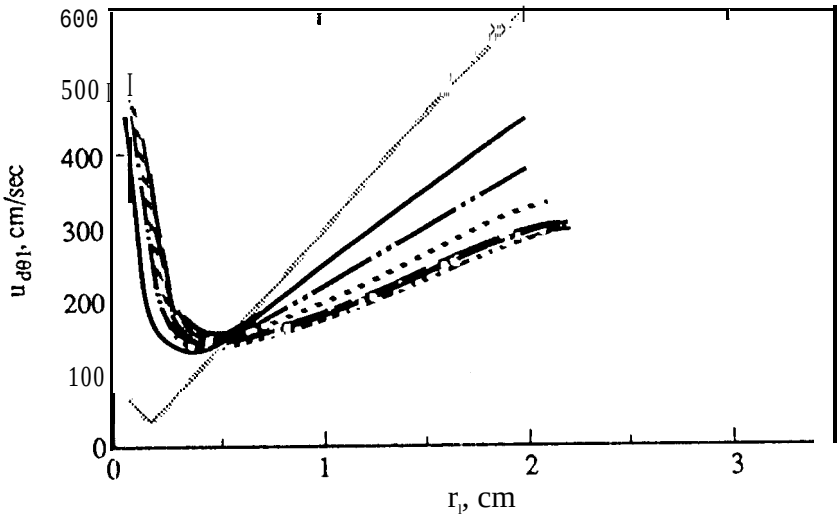

Figure 1 lb (ii)

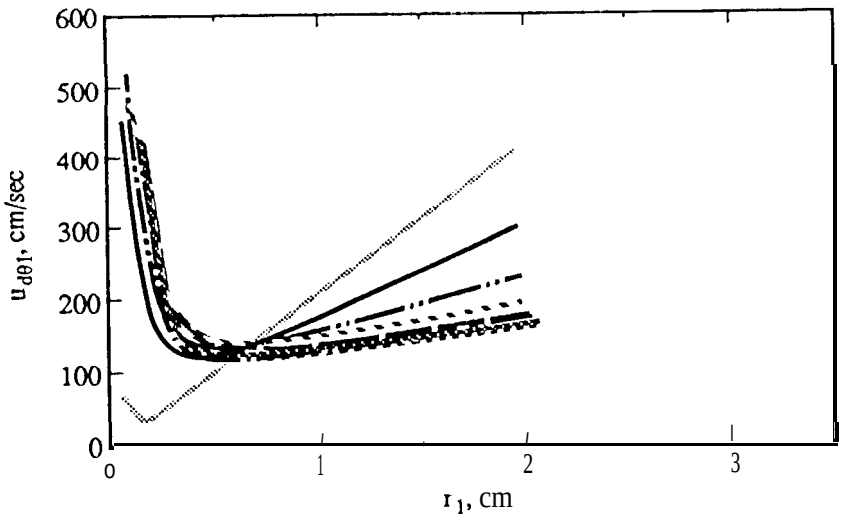

Figure 1 lb (iii)

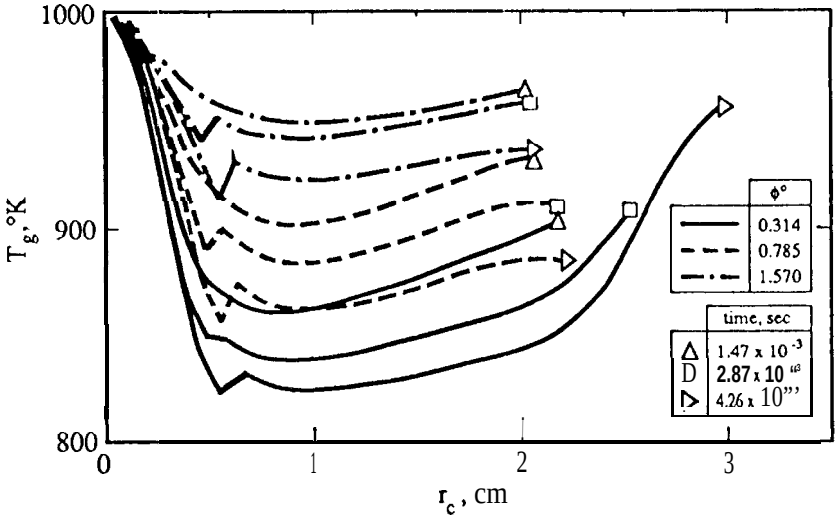
1000
900
800
0
1
2
3
T_g, °K
r_c, cm
ϕ°
0.314
0.785
1.570
time, sec
1.47 x 10 -3
2.87 x 10
4.26 x 10"'

Figure 12

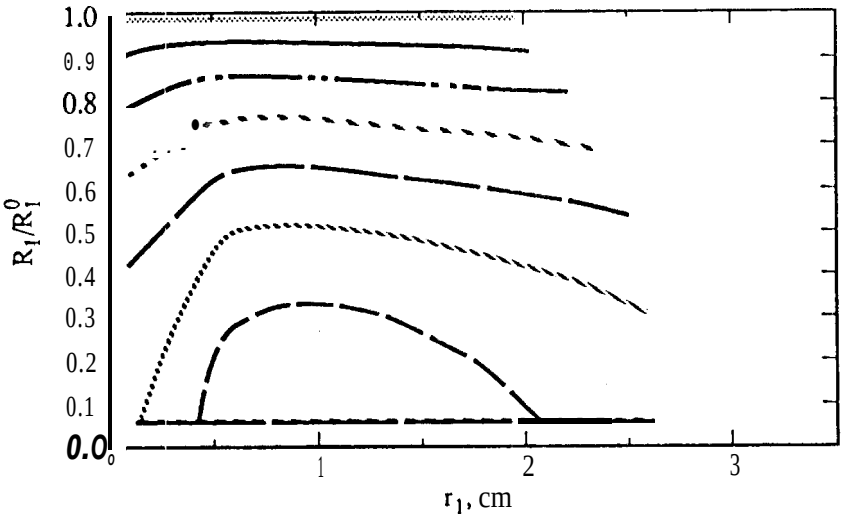

Figure 13a (i)

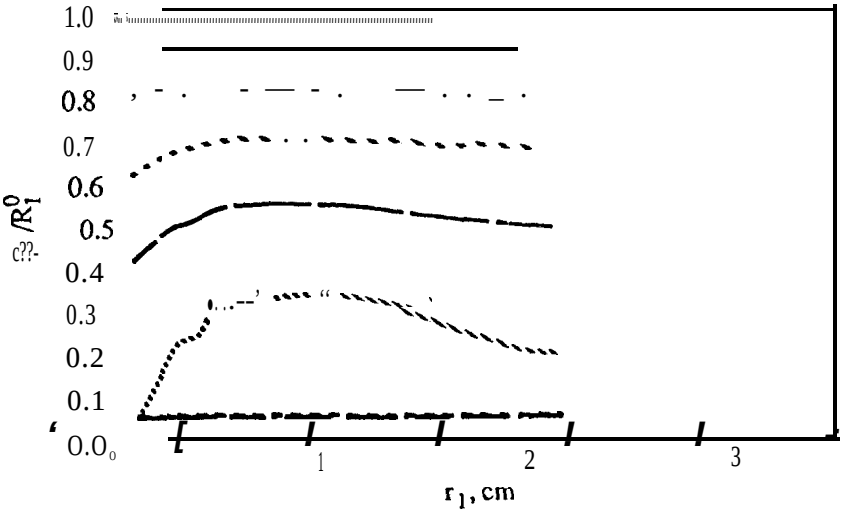

Figure 13a (ii)

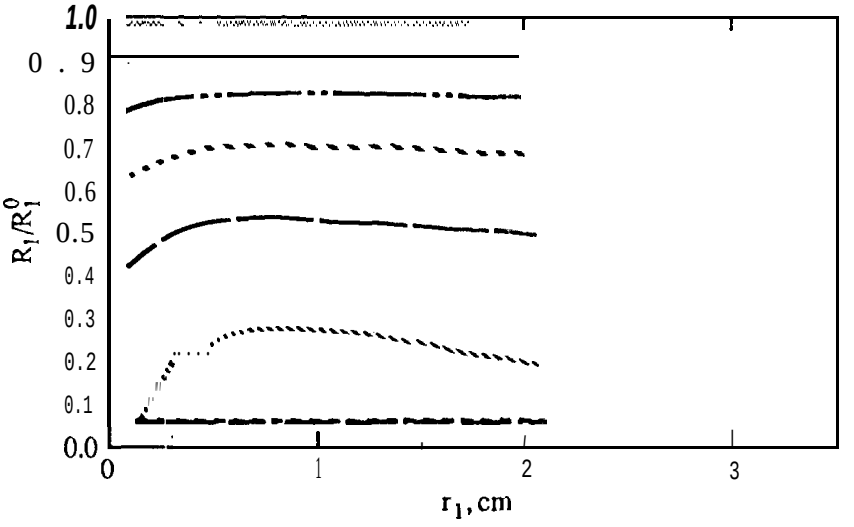

Figure 13a (iii)

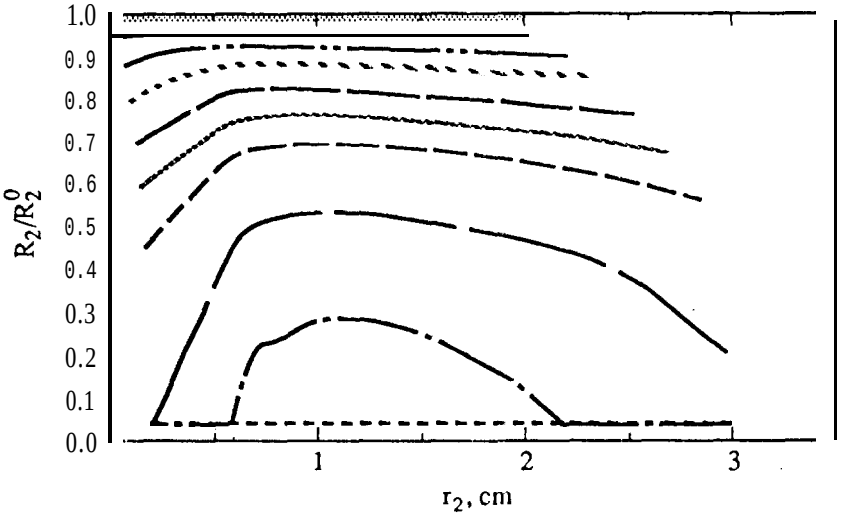

Figure 13b (i)

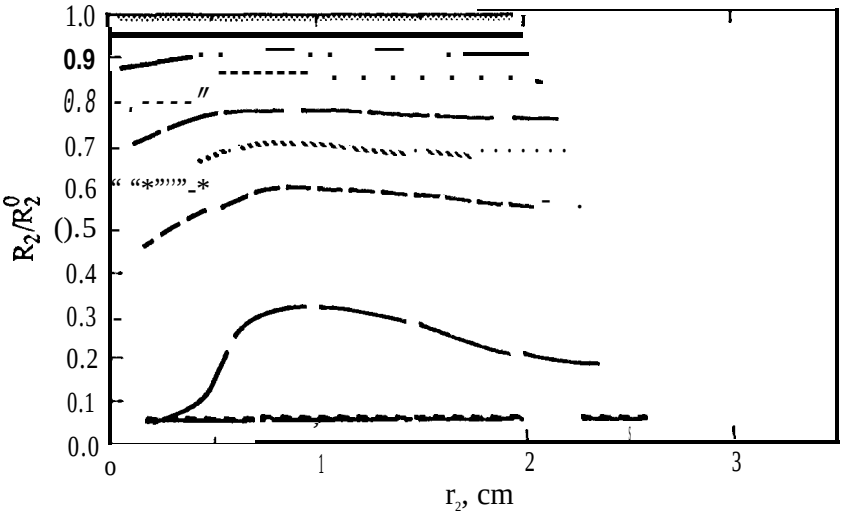

Figure 13b (ii)

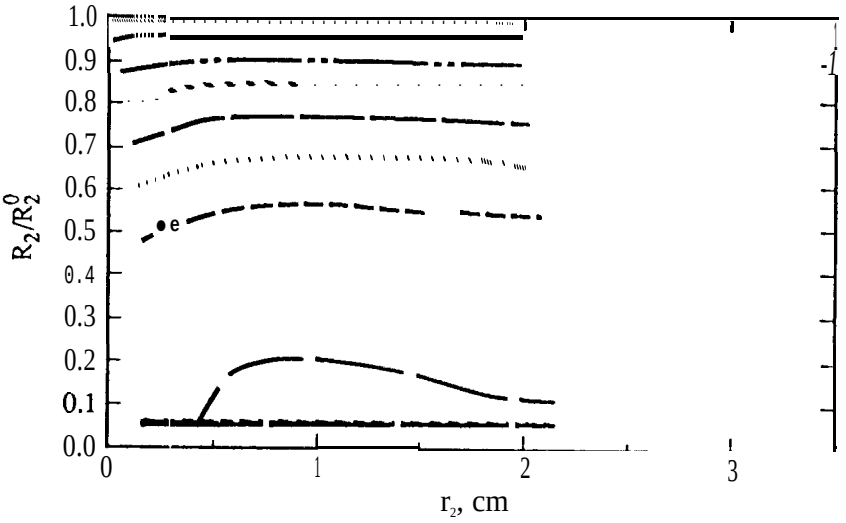

Figure 13b (iii)

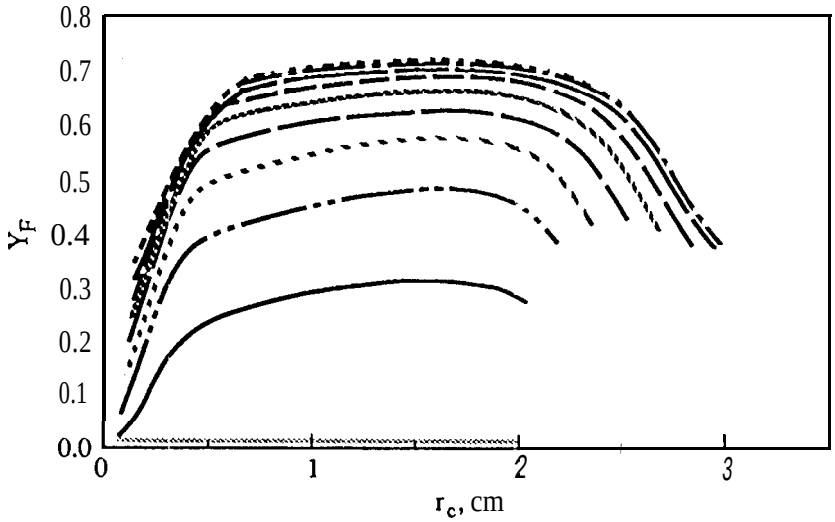

Figure 14a

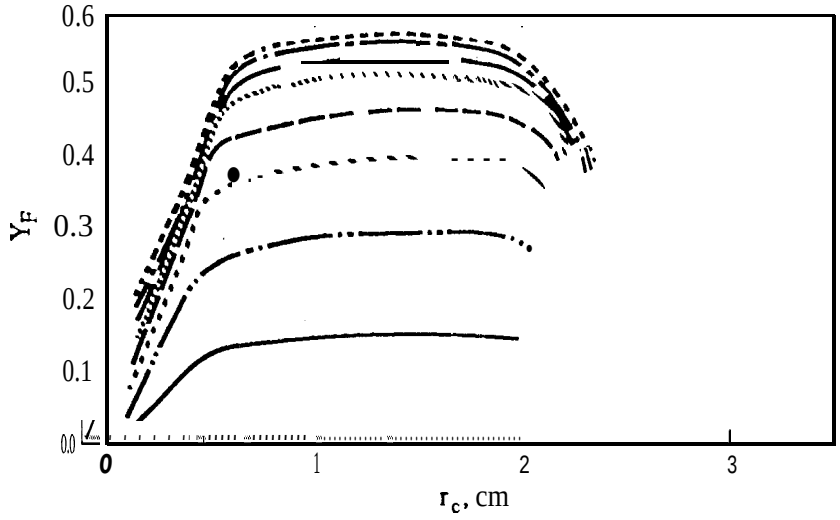

Figure 14b

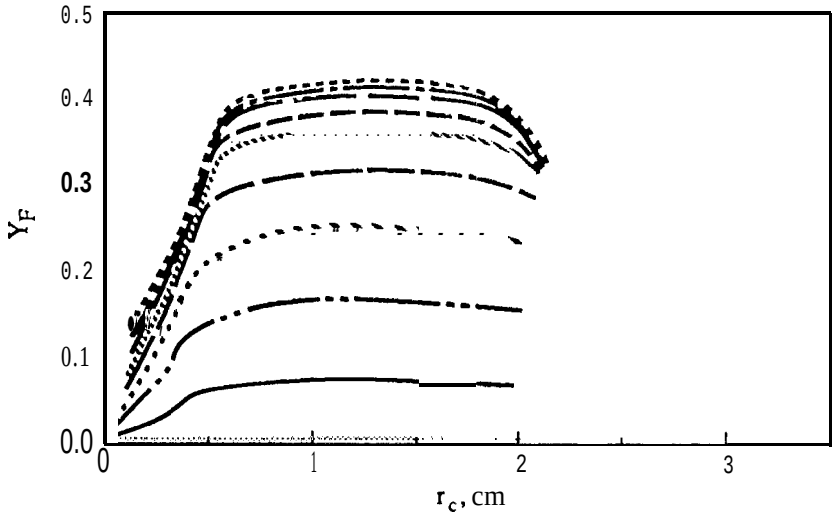

Figure 14c

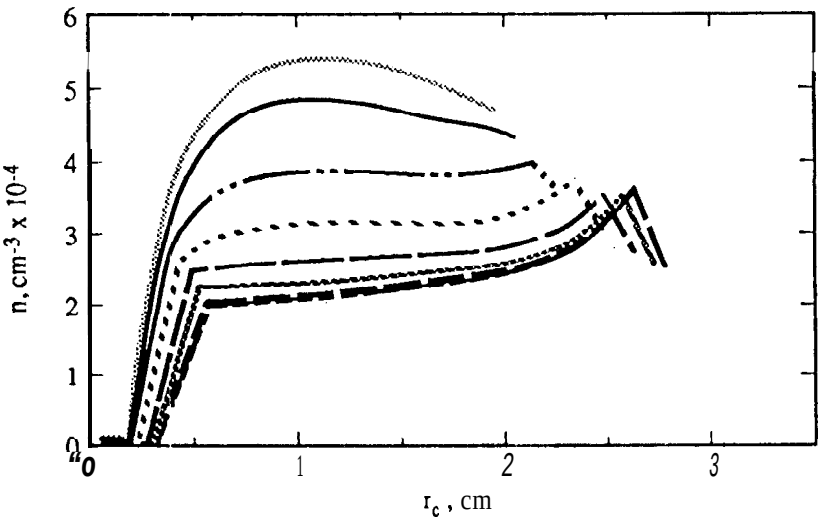

Figure 15

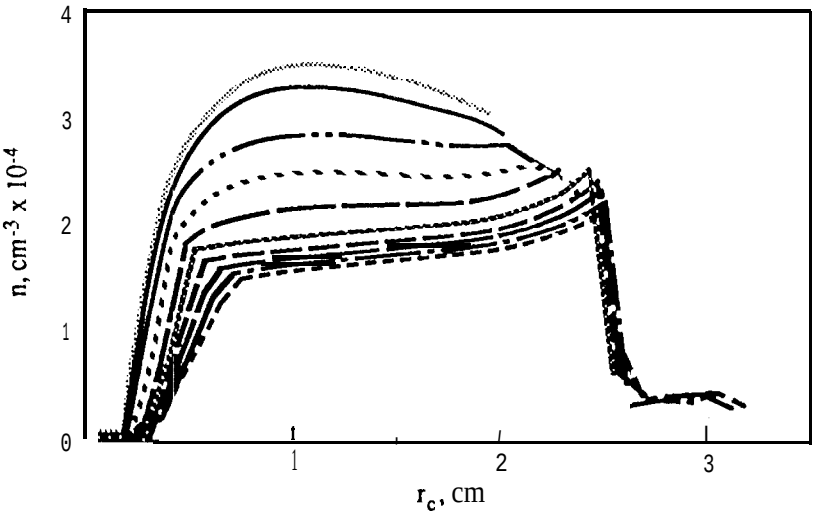

Figure 16a

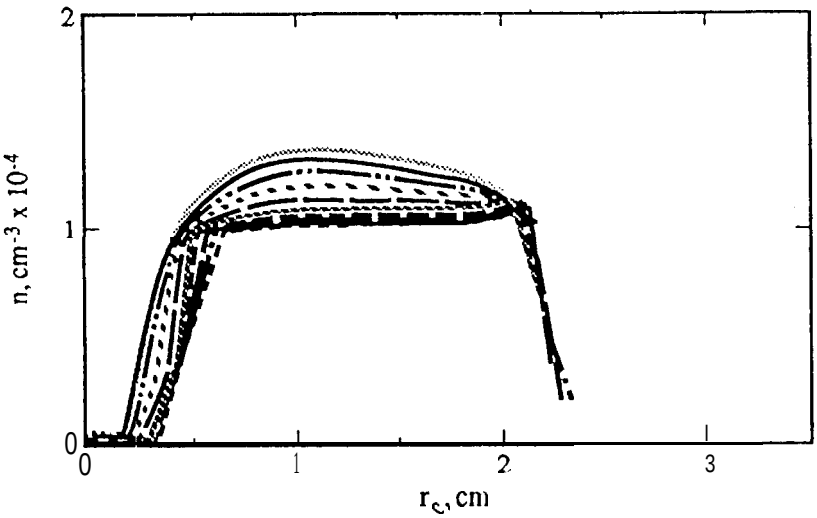

Figure 16b

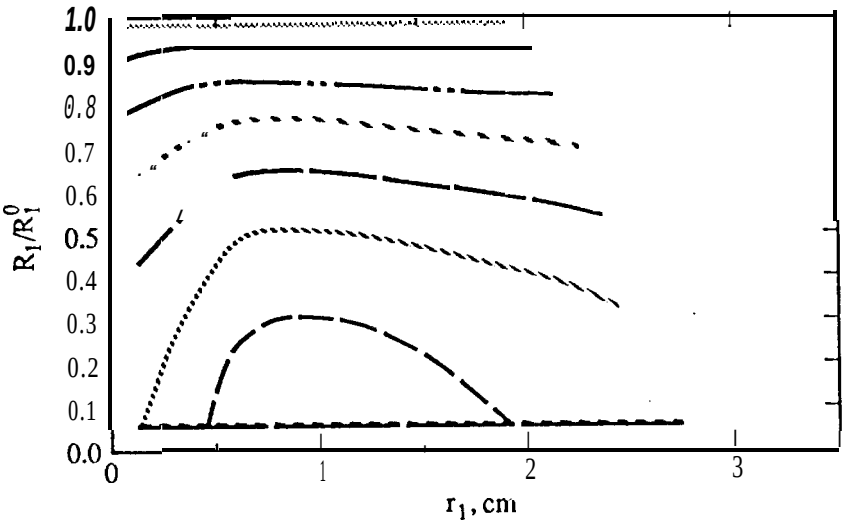

Figure 17a

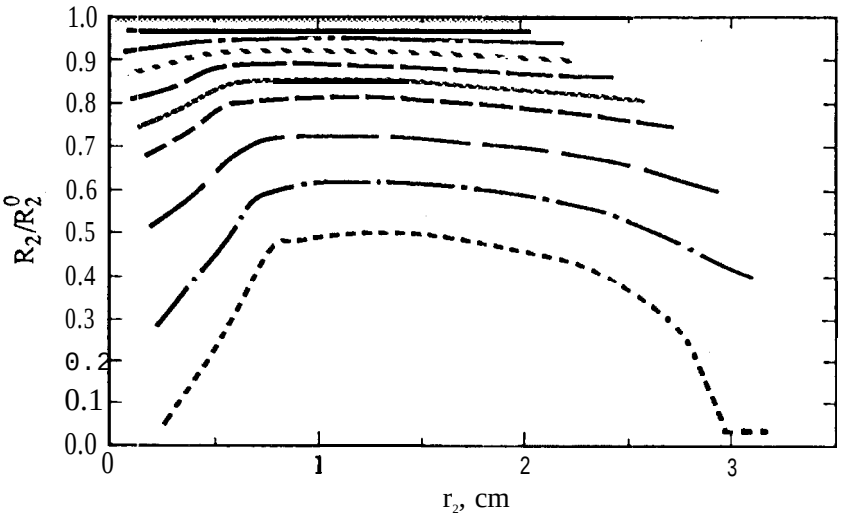

Figure 17b

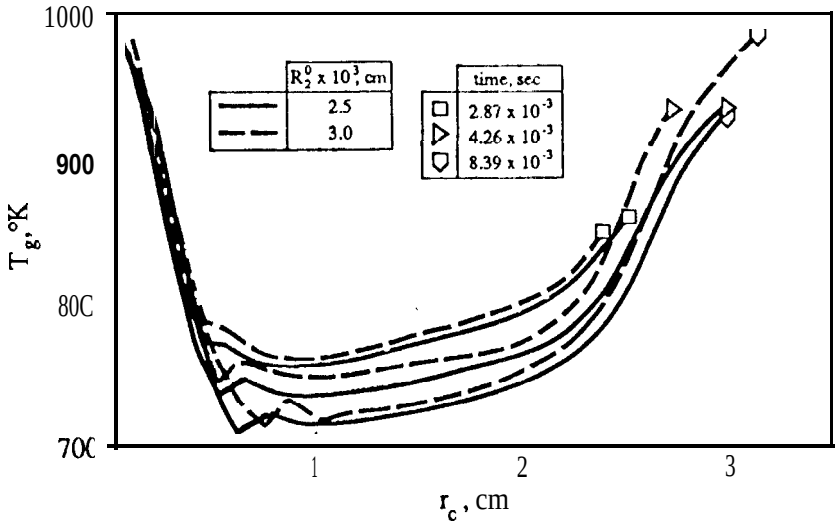
1000
900
80C
70C
T_g, °K
1
2
3
r_c, cm
$R_2^0 \times 10^3$, cm
2.5
3.0
time, sec
2.87 x 10^{-3}
4.26 x 10^{-3}
8.39 x 10^{-3}

Figure 18

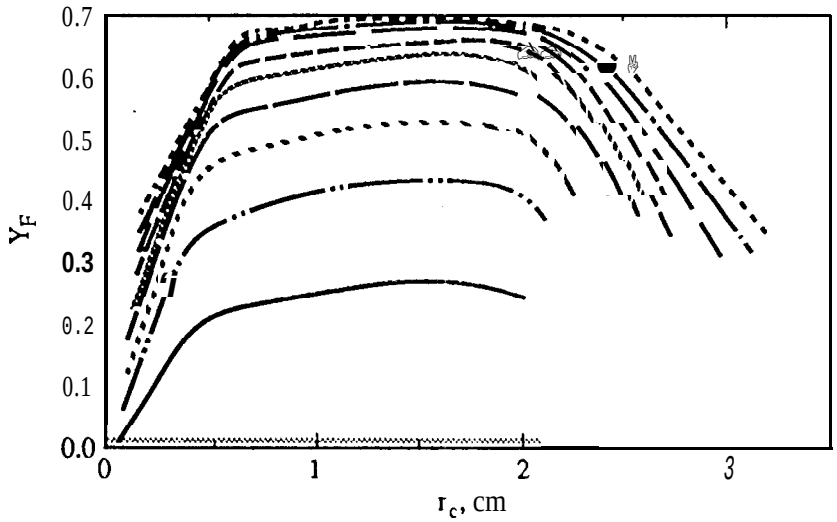

Figure 19

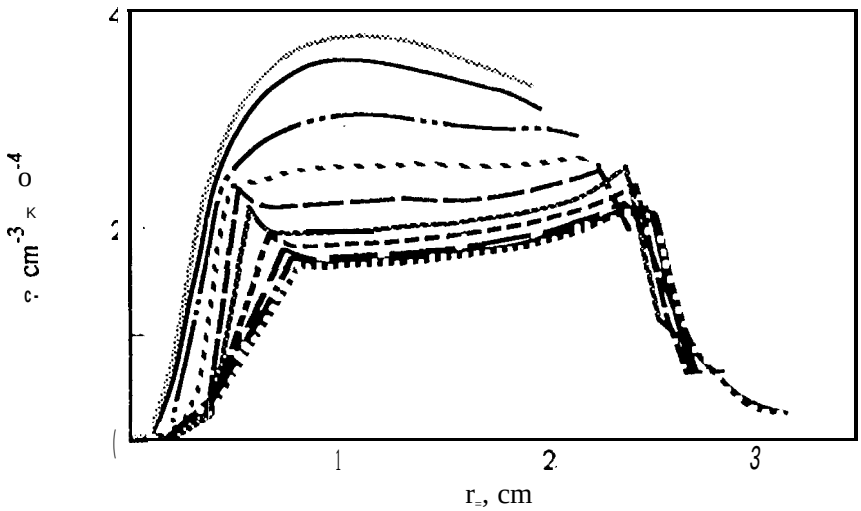

Figure 20a

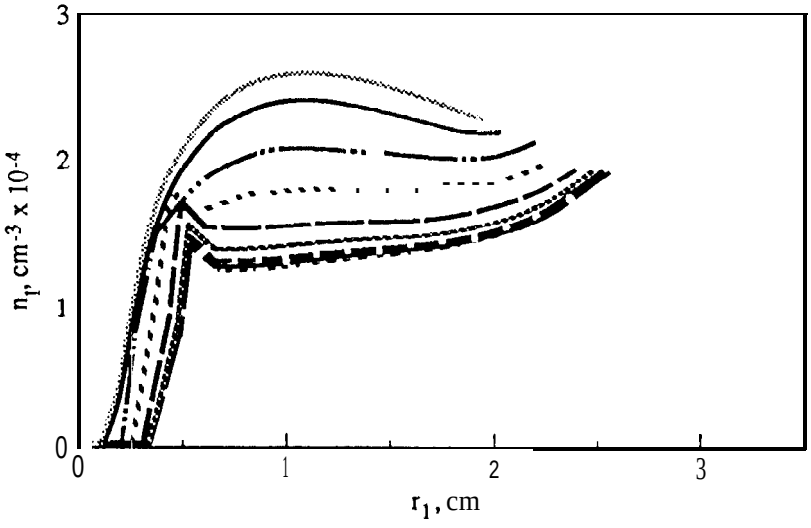

Figure 20b

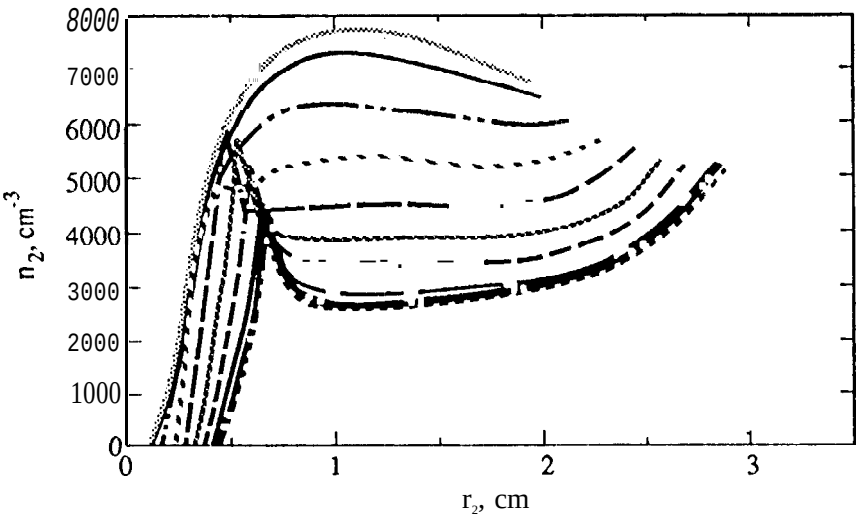

Figure 20c

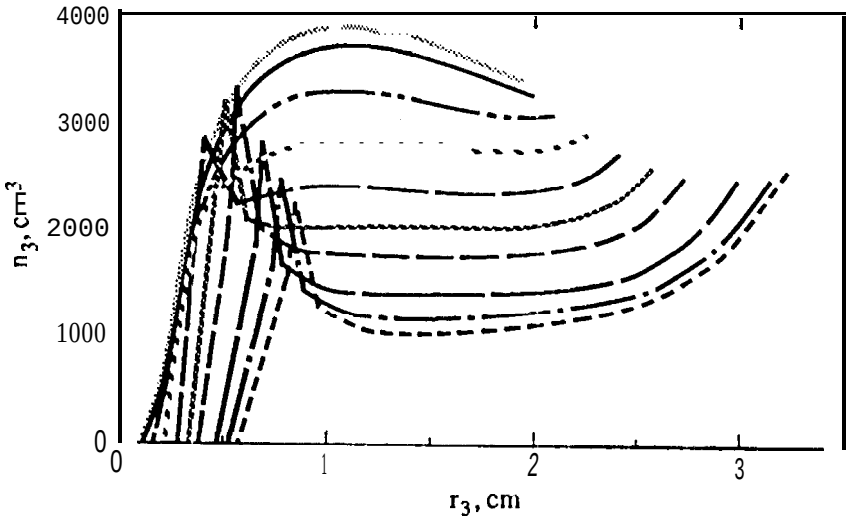

Figure 2(M

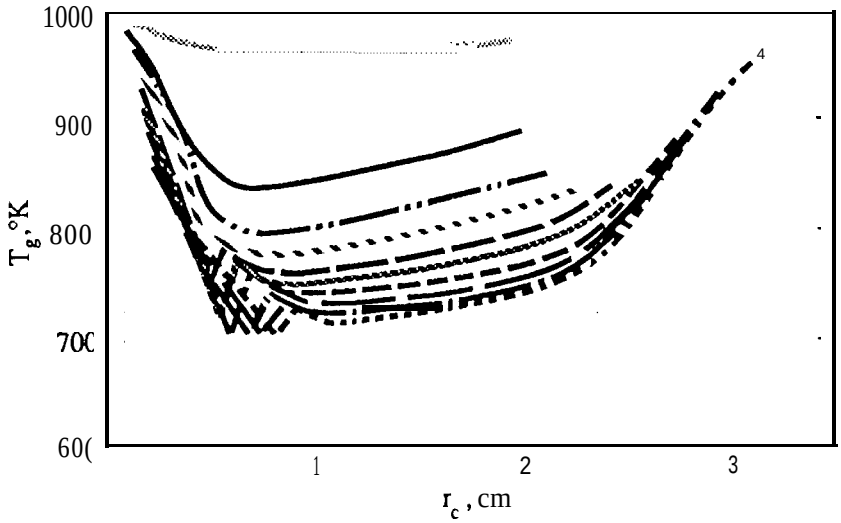

Figure 21

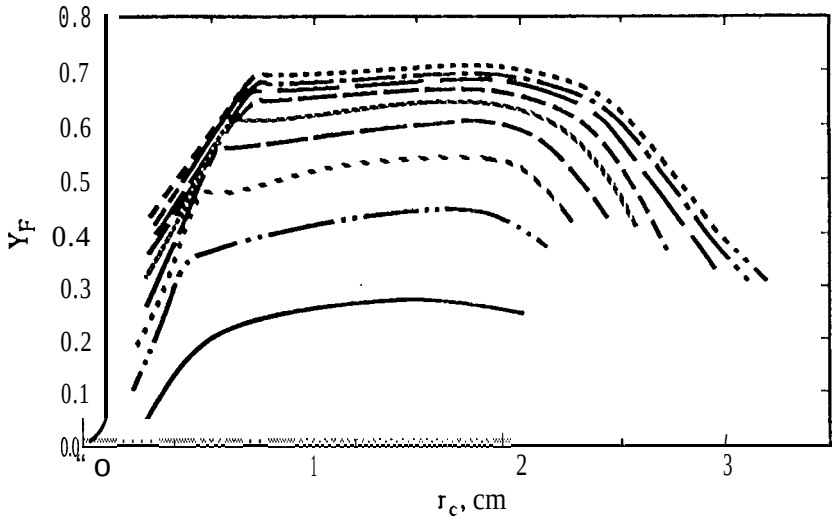

Figure 22

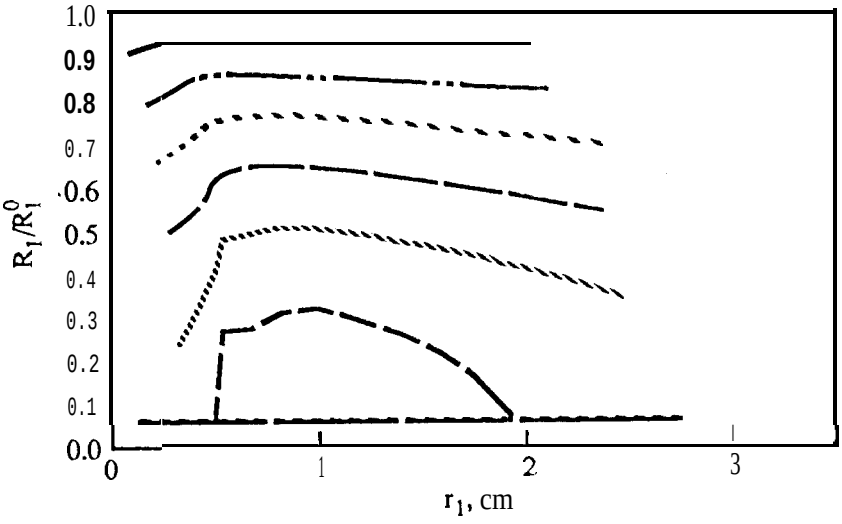

Figure 23a

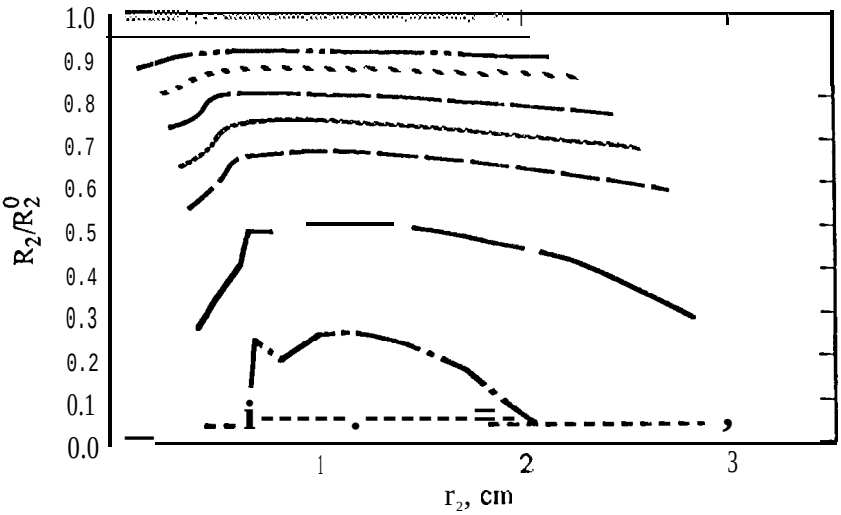

Figure 23b

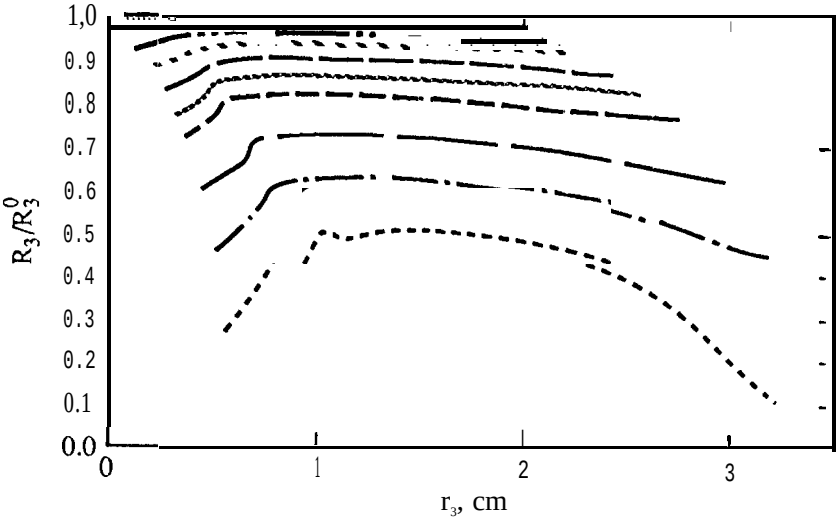

Figure 23c

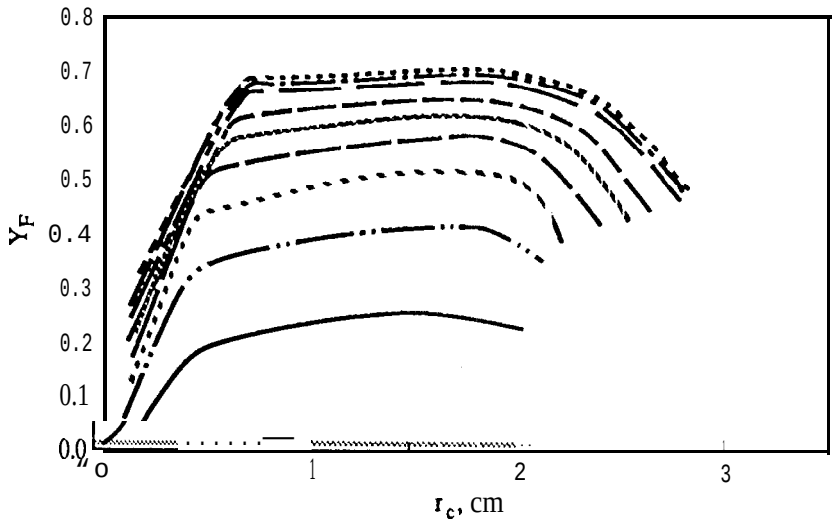

Figure 24

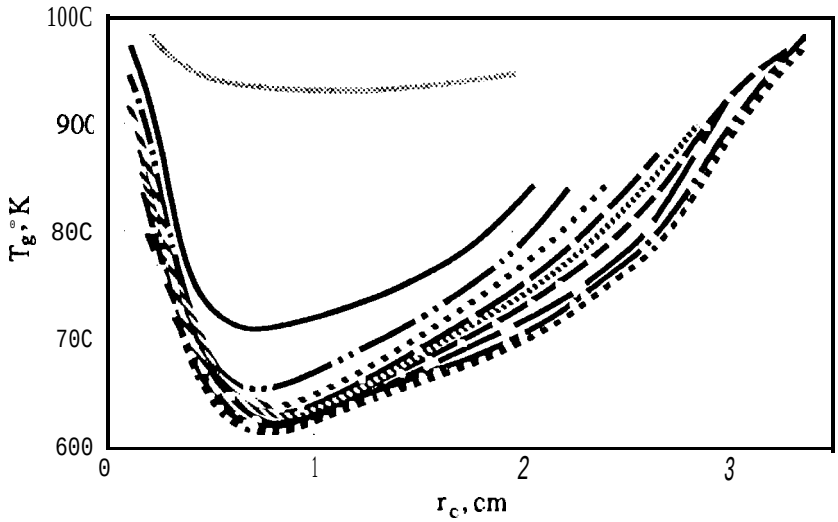

Figure 25

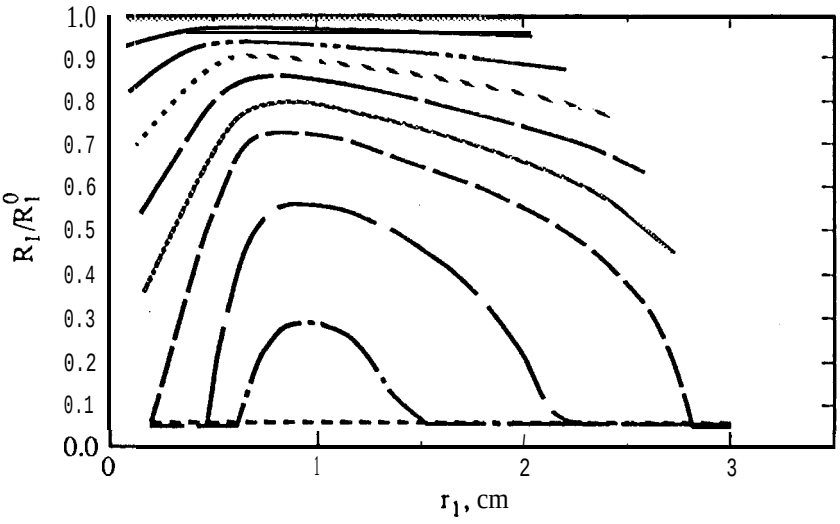

Figure 26a

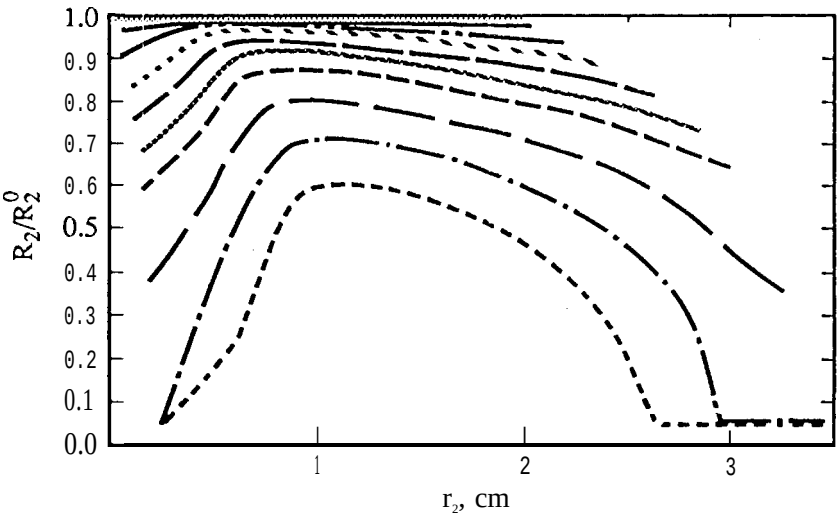

Figure 26b

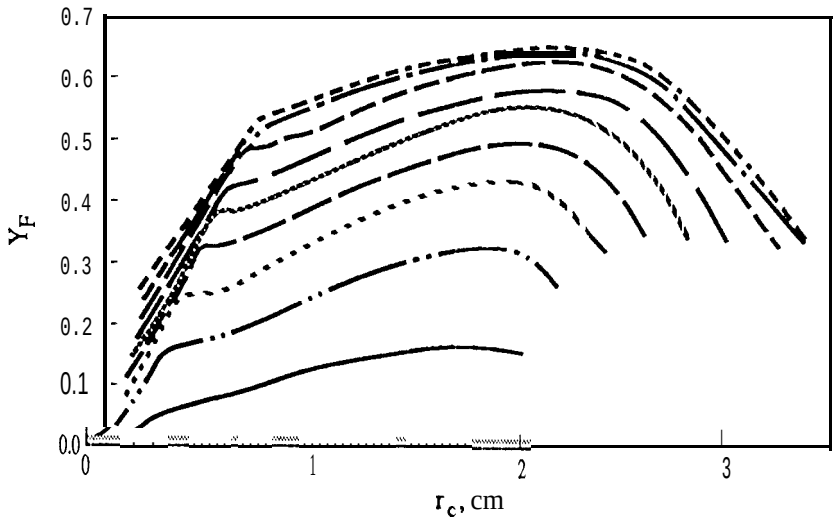

Figure 27

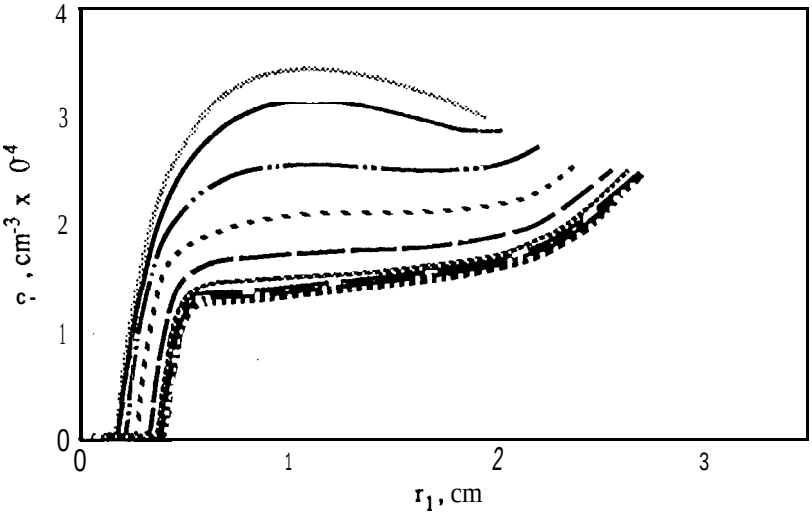

Figure 2.8a

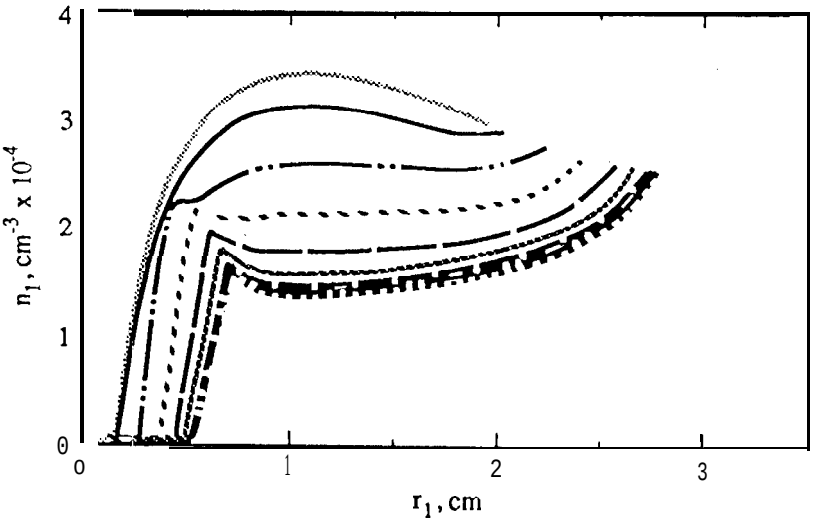

Figure 28b

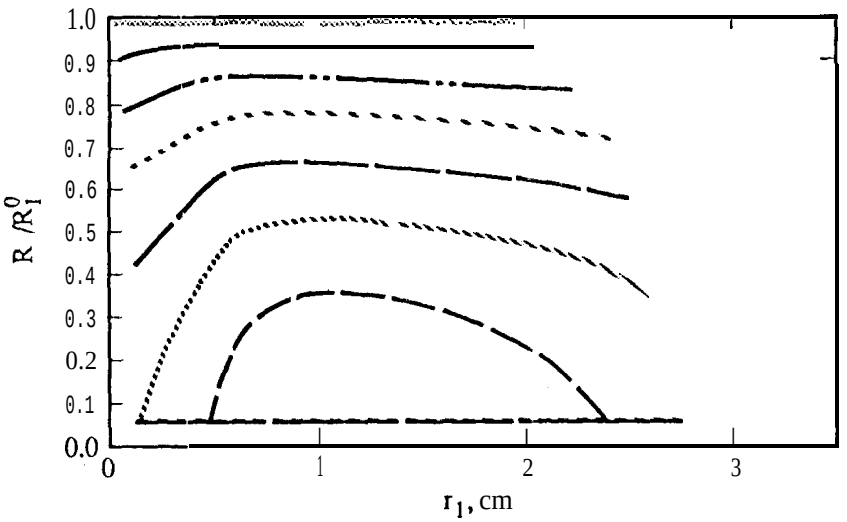

Figure 28c

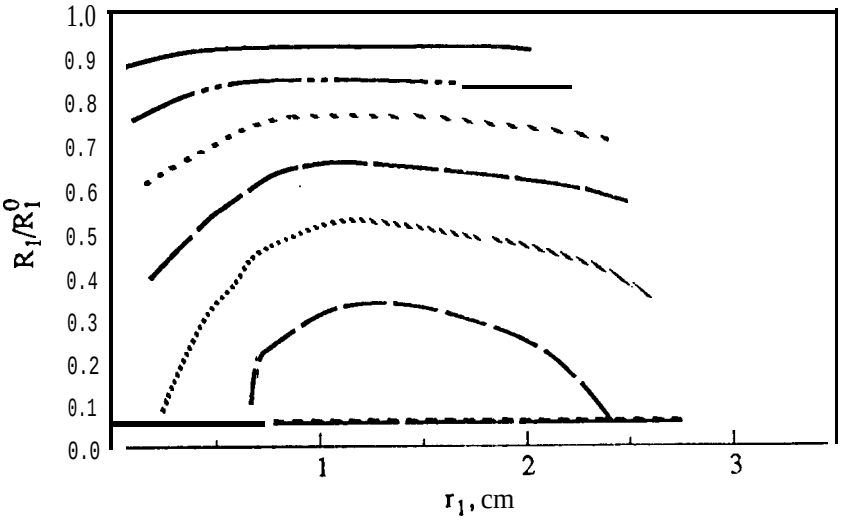

Figure 28d

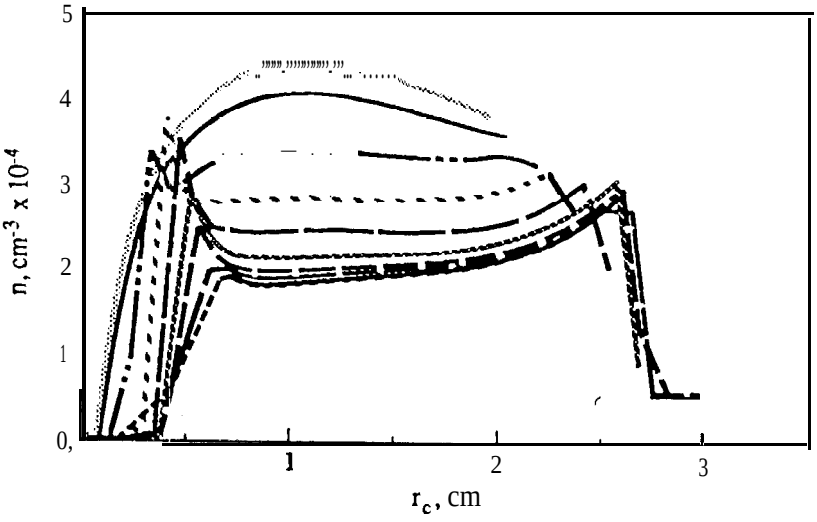

Figure 29a

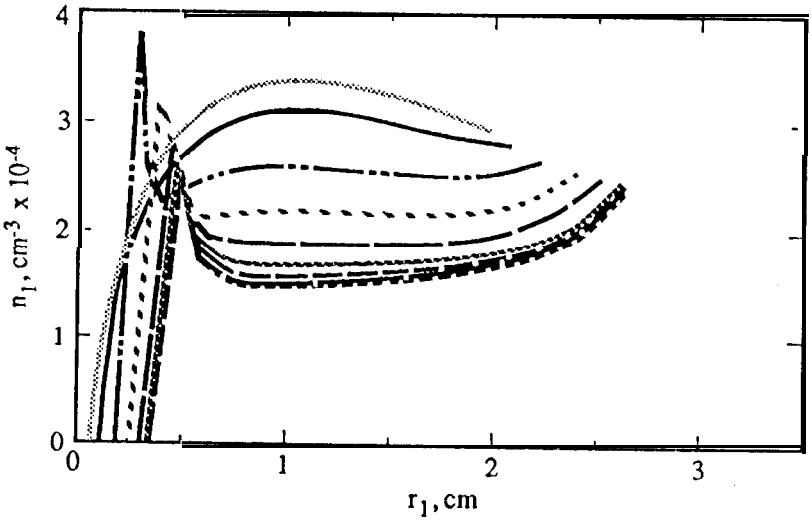

Figure 29b

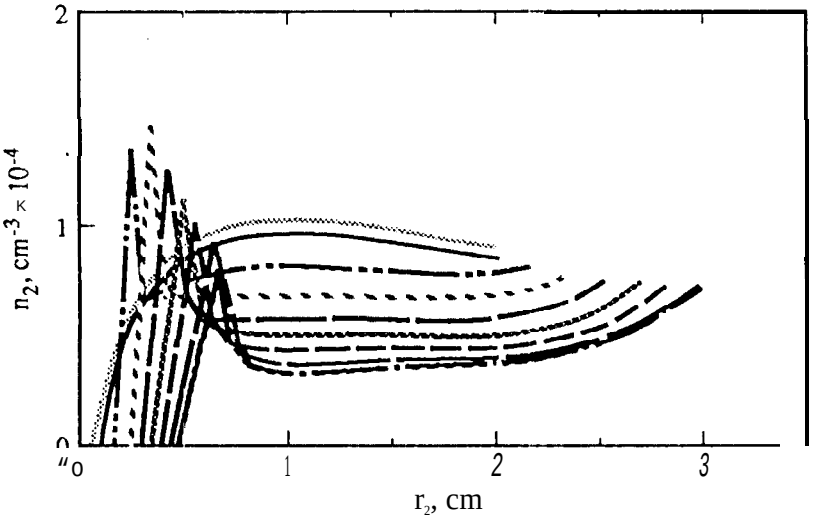

Figure 29c

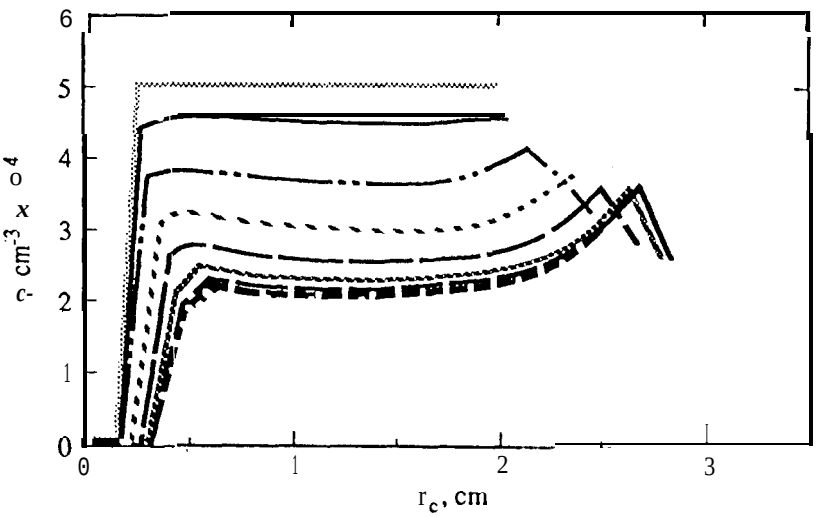

Figure 30a

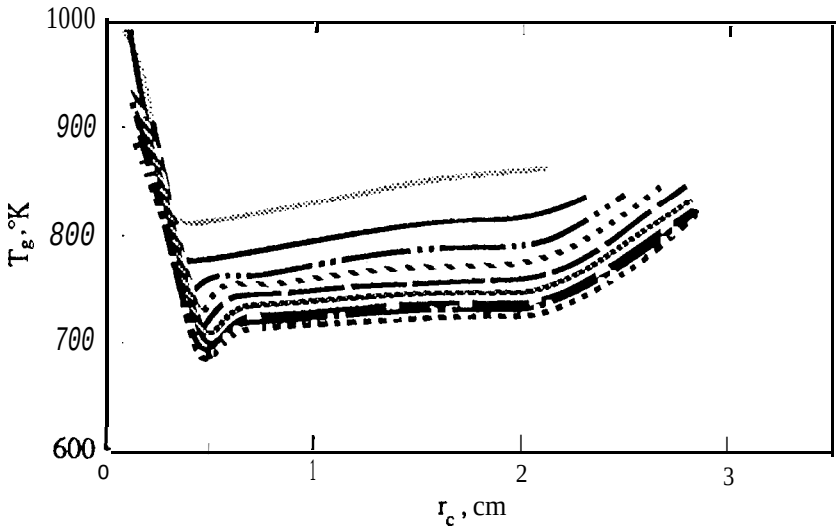

Figure 30b

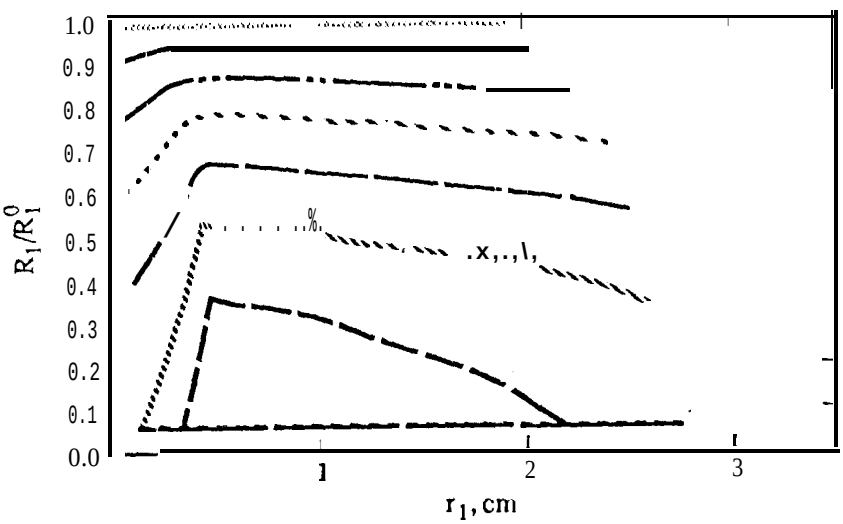

Figure 30c

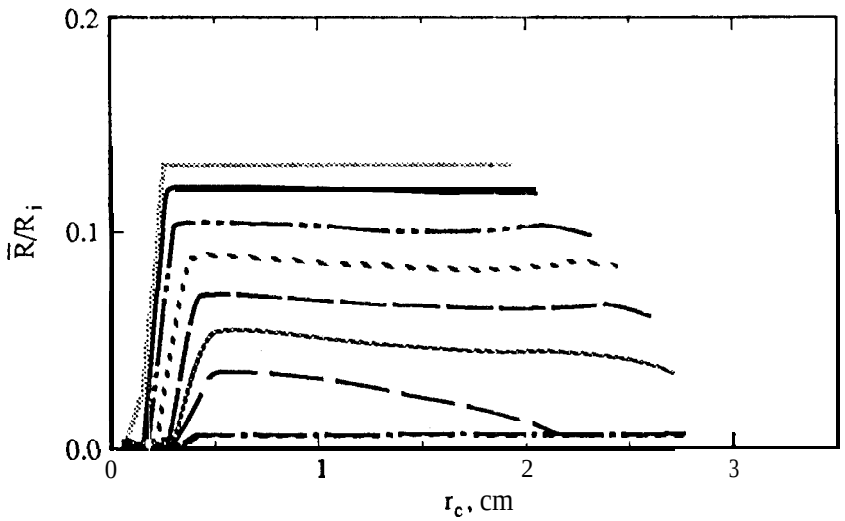

Figure 30d

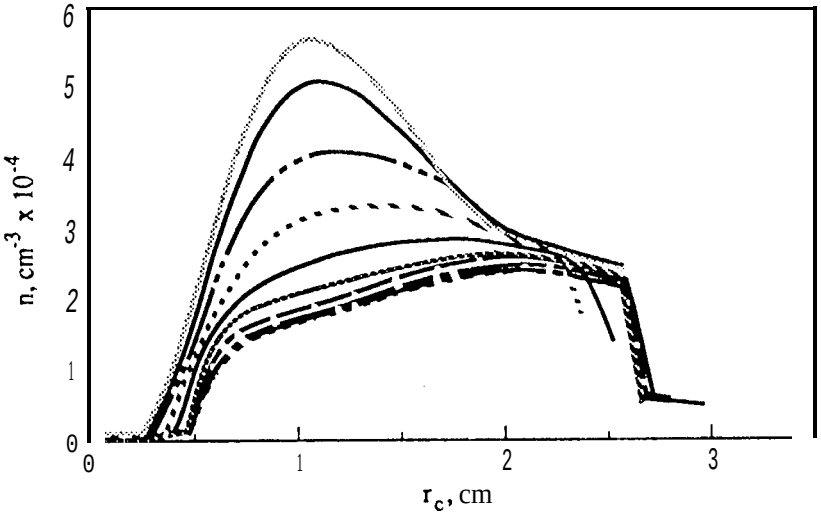

Figure. 3 la

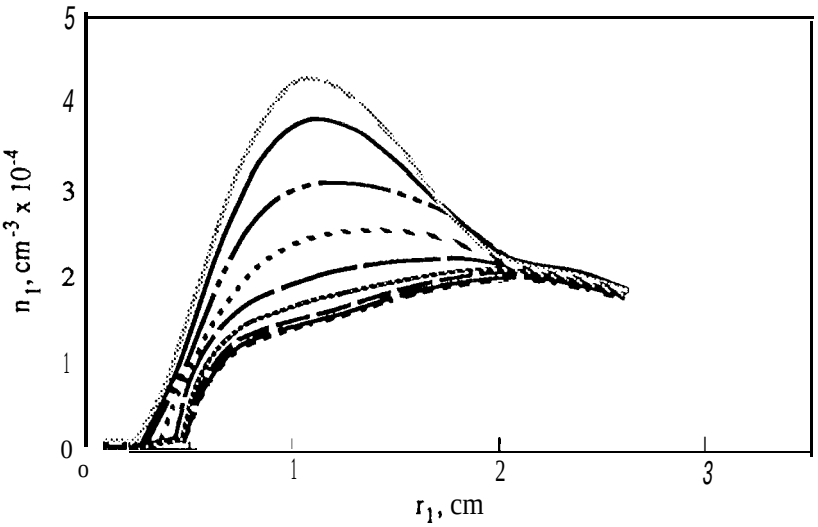

Figure 3 lb

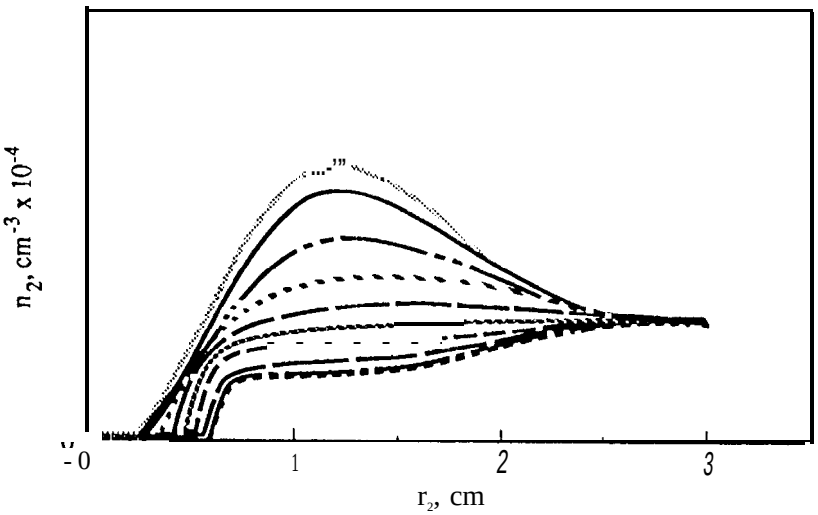

Figure 31c

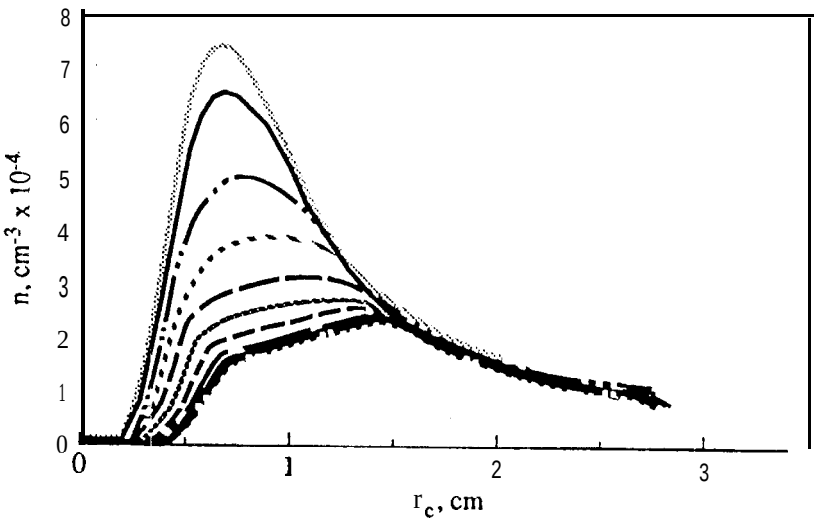

Figure 32a

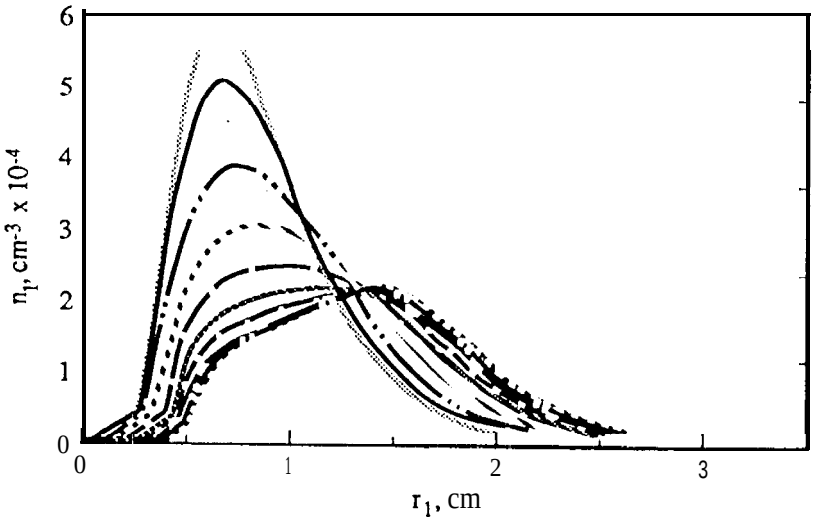

Figure 32b

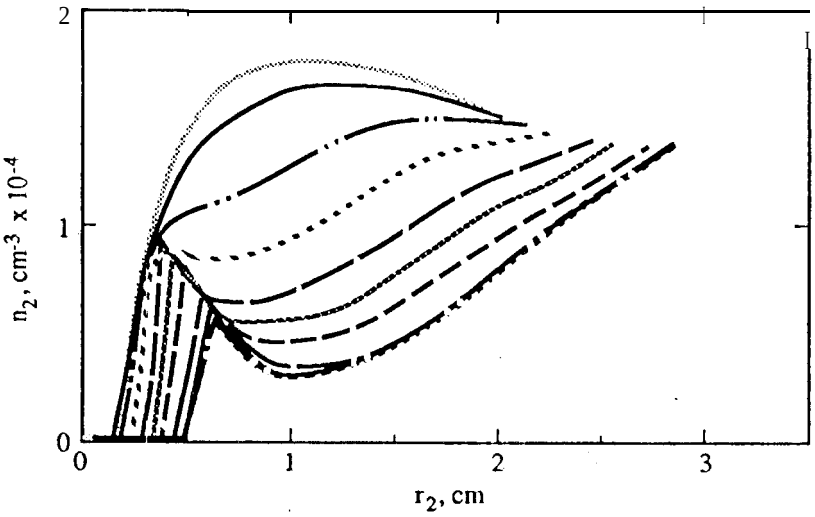

Figure 32c

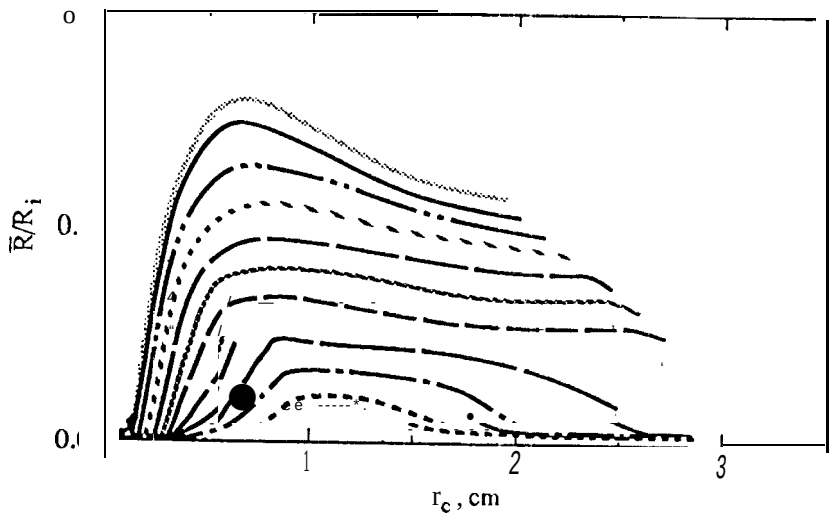

Figure 33a

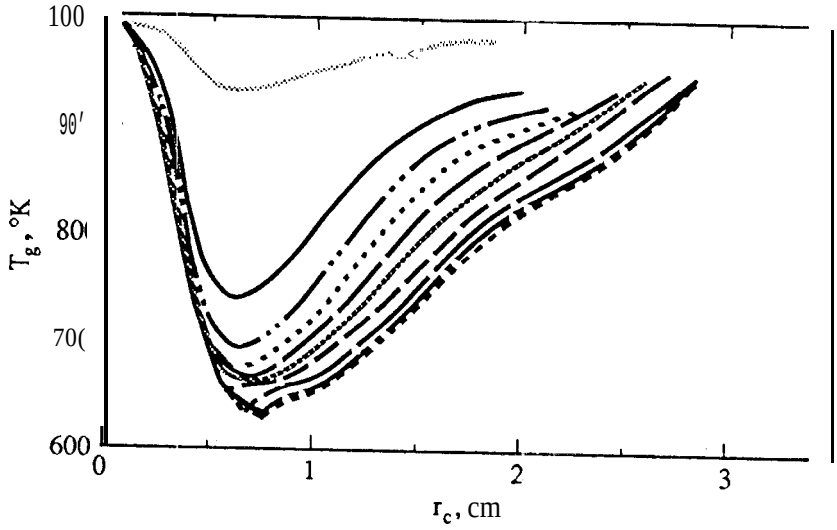

Figure 33b

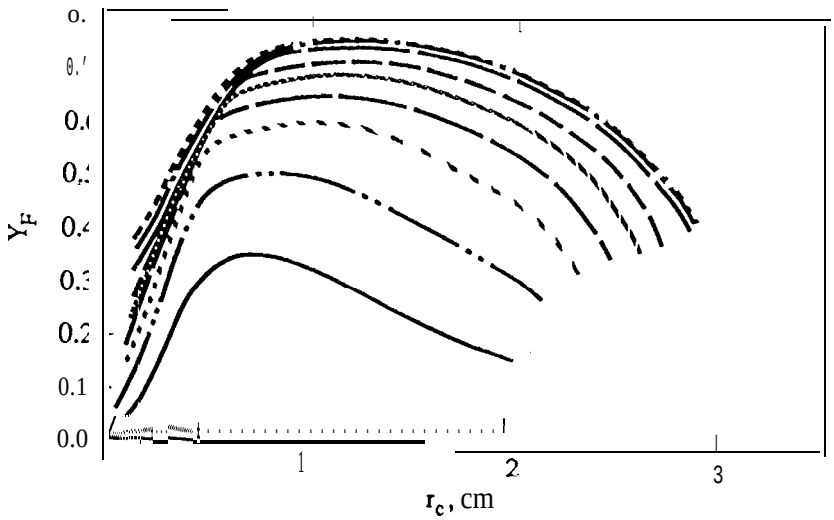

Figure 33c

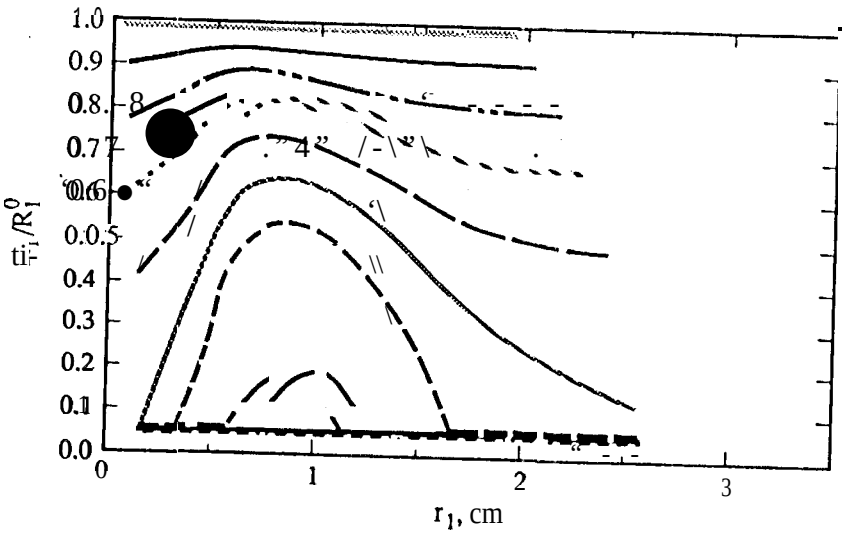

Figure 34a

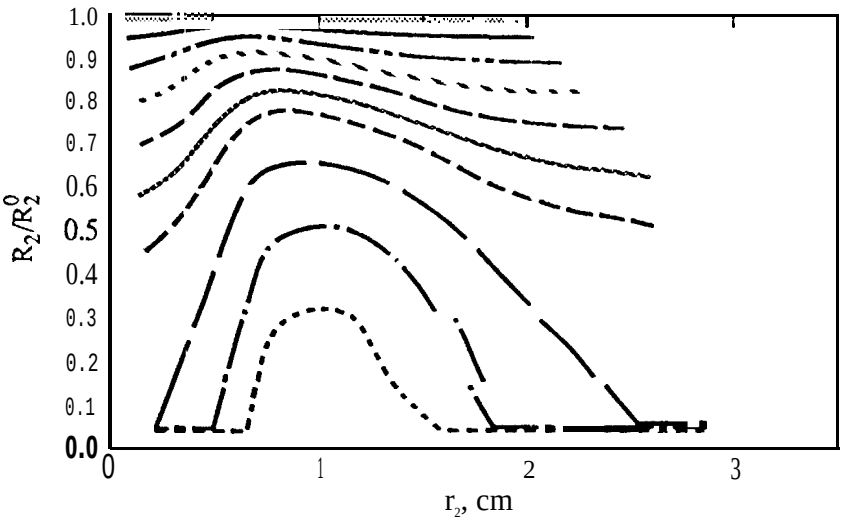

Figure 34b